Theory of *ab initio* downfolding with arbitrary-range electron-phonon coupling

Norm M. Tubman,[1,*] Christopher J. N. Coveney,[2] Chih-En Hsu,[3,4] Andres Montoya-Castillo,[5] Marina R. Filip,[2] Jeffrey B. Neaton,[6,7,8] Zhenglu Li,[4] Vojtech Vlcek,[9,10] and Antonios M. Alvertis[11,12,13,†]

[1]*NASA Ames Research Center, Moffett Field, California 94035, USA*
[2]*Department of Physics, University of Oxford, Oxford OX1 3PJ, United Kingdom*
[3]*Department of Physics, Tamkang University, New Taipei City 251301, Taiwan*
[4]*Mork Family Department of Chemical Engineering and Materials Science, University of Southern California, Los Angeles, California 90089, USA*
[5]*Department of Chemistry, University of Colorado Boulder, Boulder, Colorado 80309, USA*
[6]*Materials Sciences Division, Lawrence Berkeley National Laboratory, Berkeley, California 94720, USA*
[7]*Department of Physics, University of California, Berkeley, Berkeley, California 94720, USA*
[8]*Kavli Energy NanoScience Institute at Berkeley, Berkeley, California 94720, USA*
[9]*Materials Department, University of California, Santa Barbara, California 93106-9510, USA*
[10]*Department of Chemistry and Biochemistry, University of California, Santa Barbara, California 93106, USA*
[11]*KBR, Inc., NASA Ames Research Center, Moffett Field, California 94035, USA*
[12]*Department of Physics, The University of Texas at Austin, Austin, Texas 78712, USA*
[13]*Oden Institute for Computational Engineering and Sciences, The University of Texas at Austin, Austin, Texas 78712, USA*

(Received 7 February 2025; revised 30 April 2025; accepted 21 May 2026; published 24 June 2026)

Ab initio downfolding describes the electronic structure of materials within a low-energy subspace, often around the Fermi level. Typically starting from mean-field calculations, this framework allows for the calculation of one- and two-electron interactions, and the parametrization of a many-body Hamiltonian representing the active space of interest. The subsequent solution of such Hamiltonians can provide insights into the physics of strongly correlated materials. While phonons can substantially screen electron-electron interactions, electron-phonon coupling has been commonly ignored within *ab initio* downfolding, and when considered, this is done only for short-range coupling. Here we propose a theory of *ab initio* downfolding that accounts for short- and long-range electron-phonon coupling on equal footing. Our practical computational implementation is readily compatible with current downfolding approaches. We apply our approach to polar materials MgO and GeTe, and we reveal the importance of both short-range and long-range electron-phonon coupling in determining the magnitude of electron-electron interactions. Our results show that in the static limit, phonons reduce the on-site repulsion between electrons by 40% for MgO and by 79% for GeTe. Our framework also predicts that overall attractive nearest-neighbor interactions arise between electrons in GeTe, consistent with superconductivity in this material.

DOI: 10.1103/7hqv-hn2v

I. INTRODUCTION

Understanding the properties of materials with strong electronic correlations is a central challenge of condensed matter physics. Strong correlations are often primarily present within a low-energy subspace around the Fermi level, and can be described using so-called downfolding schemes [1–7]. Within these approaches, an accurate many-body representation of the material is derived within the subspace, typically from first-principles calculations. The high-energy electrons outside the subspace are treated at a lower level of theory, such as mean-field approaches that include density functional theory (DFT). A general Hamiltonian describing the electronic system within an active space is of the form

$$H = \sum_{ij\sigma} t_{ij} a_i^{\sigma\dagger} a_j^{\sigma} + \frac{1}{2} \sum_{ijkl\sigma\rho} U_{ijkl} a_i^{\sigma\dagger} a_j^{\rho\dagger} a_l^{\rho} a_k^{\sigma}, \tag{1}$$

where σ, ρ are spin indices, and i, j, k, l run over the electronic basis states of the system. The one-body terms t_{ij} represent hopping for $i \neq j$, and a chemical potential term for $i = j$. The two-body terms U_{ijkl} represent the two-body electronic interactions within the subspace. These interactions are screened by the electronic states outside the subspace and their magnitude may be written as $U_{ijkl} = \int d\mathbf{r} \int d\mathbf{r}' \phi_i^*(\mathbf{r})\phi_j(\mathbf{r}) W^{\mathrm{el}}(\mathbf{r}, \mathbf{r}', \omega)\phi_k^*(\mathbf{r}')\phi_l(\mathbf{r}')$, where W^{el} is the frequency-dependent electronically screened Coulomb interaction, and ϕ denotes the electronic basis states. In the context of downfolding, W^{el} is usually obtained within the constrained random-phase approximation (cRPA) [8–10].

*Contact author: norman.m.tubman@nasa.gov
†Contact author: antonios.alvertis@oden.utexas.edu

The ground and excited state properties of downfolded Hamiltonians have been successfully obtained through a variety of methods, including exact diagonalization [11,12], quantum Monte Carlo [13], and variational quantum eigensolvers [14,15]. Downfolding methods have yielded insights into the ground state properties of a variety of strongly-correlated materials, including high-temperature superconductors [3,16–19], excitonic insulators [15,20], charge-ordered systems [21,22], and beyond, as well as into the excited state properties in molecular materials [10,14].

Despite the above successes of *ab initio* downfolding approaches, the vast majority of studies in this context only consider electronic effects within Hamiltonians of the form of Eq. (1). However, it is established by this point that lattice vibrations (phonons) can renormalize the electronic properties of solids, such as their band gap [23–25], excited state energies [26–28], electron-electron interactions [29,30], and beyond. Indeed, some studies have introduced electron-phonon coupling effects within a downfolding context [22,31–34]. Specifically, Ref. [32] included the effect of short-range electron-phonon coupling from a single optical phonon on the downfolded Hamiltonian. Reference [31] developed constrained density functional perturbation theory (cDFPT), as a means of appropriately screening the properties of phonons within the subspace without double-counting interactions. Reference [31] also derived expressions for electronic interactions mediated by short-range coupling to phonons, and subsequent works have shown that this coupling can cause up to 27% reduction of the on-site electron-electron repulsion, in systems that are predicted to be metallic by DFT [35]. Reference [33] explored the implications of using cDFPT schemes for the phonon properties of molecular systems, while Ref. [22] demonstrated the potential of using downfolded electron-ion Hamiltonians to efficiently drive molecular dynamics simulations. Moreover, Ref. [34] provided a detailed investigation of how different approaches to screening affect phonon properties, and provided evidence that a combination of the cRPA and cDFPT schemes is appropriate for the downfolding of electron-phonon systems on a subspace, without introducing double-counting errors.

Despite this progress, a theoretical framework that accounts for arbitrary-range electron-phonon coupling on the downfolded electronic Hamiltonian is still missing. The formulations outlined above only account for the effect of *short-range* electron-phonon coupling on electronic interactions. While this can be appropriate in metallic systems and nonpolar semiconductors and insulators, polar, long-range electron-phonon coupling is not only important in the most general case, but can in fact dominate the electron-phonon interactions in a wide range of systems [36,37]. Several of the systems within this category exhibit strong electronic interactions near the Fermi level, and the rigorous application of downfolding frameworks could greatly improve our microscopic understanding of their physics.

Here we develop a theory of *ab initio* downfolding that includes short- and long-range coupling between electrons and phonons on equal footing. We derive expressions that allow us to quantify the effect of phonons on electron-electron interactions of arbitrary range. We formulate our theoretical approach in the basis of maximally localized Wannier functions [38], making it immediately compatible with current approaches for downfolding electronic degrees of freedom, and allowing us to present an efficient computational implementation. We apply our formalism to semiconducting MgO and GeTe, and show that apart from the previously discussed renormalization of the on-site Coulomb repulsion, there can be a strong influence of lattice motion on long-range electron-electron interactions as well. For MgO, phonons reduce the on-site electron-electron repulsion by 40%, primarily through the deformation potential mechanism. For GeTe, phonon screening results in attractive long-range electron-electron interactions due to the interplay of the Fröhlich, piezoelectric, and deformation potential mechanisms of electron-phonon coupling, offering a potential explanation for superconductivity in this system.

The structure of this paper is as follows. In Sec. II, we provide an overview of *ab initio* downfolding and the ingredients for its computational implementation. Section III develops our inclusion of phonon effects within *ab initio* downfolding, and gives the main theoretical results of this paper. In Sec. IV, we connect these theoretical results to the picture obtained from the Lang-Firsov transformation to a coupled electron-phonon system. Section V discusses the computational implementation of our formalism to efficiently account for phonons within *ab initio* downfolding. We show the results of our computational approach for MgO and GeTe in Sec. VII, and we conclude the paper with a discussion in Section VIII.

II. BRIEF OVERVIEW OF *AB INITIO* DOWNFOLDING

Within *ab initio* downfolding, the aim is to derive a many-body Hamiltonian of the form of Eq. (1), which represents the physics of a material within an active space—typically around the Fermi level. It is often convenient that the downfolded many-body Hamiltonian describes interactions of electrons on a lattice, making the choice of maximally localized Wannier functions as the computational basis a natural one. Denoting the ith Wannier orbital of our active space centered at lattice vector $\mathbf{R}$ as $\phi_{i\mathbf{R}}$, we can write the Hamiltonian in the case where we ignore Coulomb terms beyond density-density interactions as

$$H = \sum_{\sigma}\sum_{\mathbf{R}\mathbf{R}'}\sum_{ij} t_{i\mathbf{R}j\mathbf{R}'} a^{\sigma\dagger}_{i\mathbf{R}} a^{\sigma}_{j\mathbf{R}'} + \frac{1}{2}\sum_{\sigma\rho}\sum_{\mathbf{R}\mathbf{R}'}\sum_{ij} U_{i\mathbf{R}j\mathbf{R}'} a^{\sigma\dagger}_{i\mathbf{R}} a^{\rho\dagger}_{j\mathbf{R}'} a^{\rho}_{j\mathbf{R}'} a^{\sigma}_{i\mathbf{R}}. \tag{2}$$

The downfolding procedure is schematically illustrated in Fig. 1.

The one-body and two-body terms $t_{i\mathbf{R}j\mathbf{R}'}$, $U_{i\mathbf{R}j\mathbf{R}'}$ appearing in Hamiltonian of Eq. (2) are computed from first principles. The hopping term is

$$t_{i\mathbf{R}j\mathbf{R}'} = \int_V d\mathbf{r}\phi^*_{i\mathbf{R}}(\mathbf{r}) H_o \phi_{j\mathbf{R}'}(\mathbf{r}'), \tag{3}$$

where H_o a single-particle description of the electronic system, often taken to be equal to the Kohn-Sham Hamiltonian H_{KS}. The two-body Coulomb interaction is written

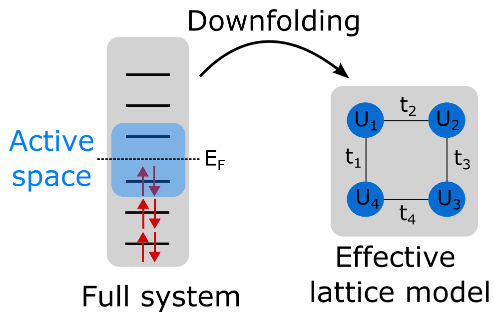

FIG. 1. Schematic illustration of *ab initio* downfolding. Starting from a description of the full system, an active space, typically around the Fermi level, is downfolded onto an effective many-body Hamiltonian on a lattice.

as [11]

$$U_{i\mathbf{R}j\mathbf{R}'}(\omega) = \int_V d\mathbf{r} \int_V d\mathbf{r}' \phi^*_{i\mathbf{R}}(\mathbf{r})\phi_{i\mathbf{R}}(\mathbf{r})W(\mathbf{r},\mathbf{r}',\omega)\phi^*_{j\mathbf{R}'}(\mathbf{r}')\phi_{j\mathbf{R}'}(\mathbf{r}'). \tag{4}$$

The frequency-dependent screened Coulomb interaction $W(\mathbf{r},\mathbf{r}',\omega)$ is commonly taken to be equal to the electronically screened Coulomb interaction, i.e., $W = W^{\text{el}}$, within the cRPA, and in those cases we denote $U = U^{\text{el}}$.

It is important to emphasize at this point that the Hamiltonian of Eq. (2) is of the extended Hubbard form and constitutes a specific choice for the representation of the electronic structure within the active space of interest. In addition to the one-body hopping and two-body Coulomb terms, a two-body exchange term is also included in some cases [11]. Moreover, it is possible to incorporate terms beyond density-density Coulomb interactions [39], as in the Hamiltonian of Eq. (1). Our theoretical framework outlined below may be readily extended to incorporate phonon effects on general four-center integrals. Due to the more cumbersome notation that this entails, we will present here our results primarily for two-center integrals, however, in Appendix A, we give the expressions for the more general case.

An important aspect of the two-body terms of Eq. (4) is the frequency dependence of the screened Coulomb interaction. This derives from the frequency dependence of the inverse dielectric matrix ϵ^{-1}, which screens the bare Coulomb repulsion v [40–42]:

$$W^{\text{el}}(\mathbf{r},\mathbf{r}',\omega) = \int d\mathbf{r}''\epsilon^{-1}(\mathbf{r},\mathbf{r}'',\omega)v(\mathbf{r}'',\mathbf{r}'), \tag{5}$$

where v the bare (unscreened) Coulomb interaction. This expression may in turn be written as [43]

$$W^{\text{el}}_{\mathbf{G}\mathbf{G}'}(\mathbf{q},\omega) = \epsilon^{-1}_{\mathbf{G}\mathbf{G}'}(\mathbf{q},\omega)v(\mathbf{q}+\mathbf{G}'), \tag{6}$$

where here we work in reciprocal space and a plane wave basis, denoting $\mathbf{q}$ as a vector within the first Brillouin zone, and $\mathbf{G}$ as a reciprocal lattice vector. Within the cRPA, the dielectric matrix is written as

$$\epsilon_{\mathbf{G}\mathbf{G}'}(\mathbf{q},\omega) = \delta_{\mathbf{G}\mathbf{G}'} - v(\mathbf{q}+\mathbf{G})\chi_{\mathbf{G}\mathbf{G}'}(\mathbf{q},\omega), \tag{7}$$

where the bare Coulomb interaction is

$$v(\mathbf{q}+\mathbf{G}) = 4\pi/|\mathbf{q}+\mathbf{G}|^2, \tag{8}$$

and the polarizability is written as

$$\begin{aligned}\chi_{\mathbf{G}\mathbf{G}'}(\mathbf{q},\omega) = {} & \sum_{\mathbf{k}}\sum_{n}^{\text{occ}}\sum_{n'}^{\text{unocc}}(1 - T_{n'\mathbf{k}+\mathbf{q}}T_{n\mathbf{k}}) \\ & \times M_{nn'}(\mathbf{k},\mathbf{q},\mathbf{G})M^*_{nn'}(\mathbf{k},\mathbf{q},\mathbf{G}') \\ & \times \left[\frac{1}{\omega - E_{n'\mathbf{k}+\mathbf{q}} + E_{n\mathbf{k}} + i\delta}\right. \\ & \left. - \frac{1}{\omega + E_{n'\mathbf{k}+\mathbf{q}} - E_{n\mathbf{k}} - i\delta}\right],\end{aligned} \tag{9}$$

where $\delta \to 0^+$. Here we sum over $\mathbf{k}$ points, occupied and unoccupied bands, and we use the notation $M_{nn'}(\mathbf{k},\mathbf{q},\mathbf{G}) = \langle n\mathbf{k}+\mathbf{q}|\, e^{i(\mathbf{q}+\mathbf{G})\cdot\mathbf{r}}\, |n'\mathbf{k}\rangle$. Moreover, we take the definition

$$T_{n\mathbf{k}} = \sum_{i}^{N_{\text{wan}}} w^{\mathbf{k}}_{\text{ni}} w^{\mathbf{k}*}_{\text{ni}}, \tag{10}$$

where we sum over the number of Wannier states in the subspace, and $w^{\mathbf{k}}_{\text{ni}}$ are the rotation matrices that take us from the plane wave to the Wannier basis [11]. The term $(1 - T_{n'\mathbf{k}+\mathbf{q}}T_{n\mathbf{k}})$ excludes the screening of the states within the subspace, hence avoiding double-counting. In regular RPA, rather than cRPA, the polarizability is computed by setting $T_{n'\mathbf{k}+\mathbf{q}}T_{n\mathbf{k}} = 0$.

A common approximation to simplify the frequency dependence of the screened Coulomb interaction is to take the static limit $\omega = 0$ in Eqs. (6), (7), and (9). This is a significant simplification; finding the eigenvalues of a downfolded Hamiltonian which includes frequency dependence constitutes a nonlinear problem [44], the accurate solution of which is an active area of research. The static approximation can lead to both underscreening and overscreening of Coulomb interactions depending on the details of a given system [39,45], nevertheless its simplicity and practicality has led to its widespread adoption. Our formalism for including phonon effects in *ab initio* downfolding, as developed in the following Sec. III, includes the full frequency dependence of phonon screening, however, we will, in some cases, discuss the static limit in order to develop intuition, and to understand the impact of our approach on results similar to those reported in the literature.

III. INCLUSION OF PHONON EFFECTS

The key element in determining the electron-electron interactions $U_{i\mathbf{R}j\mathbf{R}'}$ within a subspace is the screened Coulomb interaction W, as expressed in Eq. (4). So far, we have only considered the case where the Coulomb interaction is screened electronically, i.e., $W = W^{\text{el}}$. However, it is established that phonons can also screen the Coulomb interaction between electrons. Within many-body perturbation theory and to the lowest order in the electron-phonon interaction, the phonon correction to the screened Coulomb interaction is written as [46–48]

$$W^{\text{ph}}(\mathbf{r},\mathbf{r}',\omega) = \sum_{\mathbf{q},\nu} D_{\mathbf{q},\nu}(\omega)g_{\mathbf{q},\nu}(\mathbf{r})g^*_{\mathbf{q},\nu}(\mathbf{r}'). \tag{11}$$

Here $D_{\mathbf{q},\nu}(\omega)$ is the propagator of a phonon with branch index ν and at wavevector $\mathbf{q}$, and $g_{\mathbf{q},\nu}$ is the electron-phonon vertex.

The phonon propagator here already includes inter-phonon mixing [49] as described by a nonanalytical contribution [50]. Phonon screening can result in attractive electron-electron interactions and phenomena such as superconductivity [51], and has also recently been incorporated in the *ab initio* calculation of excited states within the *GW*-Bethe-Salpeter equation formalism [52], where it was shown that it can lead to strongly temperature- dependent exciton binding energies. Moreover, it was found in Refs. [52,53] that Fröhlich-like long-range coupling of electrons to longitudinal phonons dominates this effect in semiconductors.

We now include phonon screening in the screened Coulomb interaction appearing in Eq. (4), i.e., we take the total screened Coulomb interaction to be

$$W = W^{\mathrm{el}} + W^{\mathrm{ph}}, \tag{12}$$

where W^{el} is given by Eq. (5), and W^{ph} is given by Eq. (11). We therefore obtain the *total* Coulomb interaction

$$\begin{aligned} U^{\mathrm{tot}}_{i\mathbf{R}j\mathbf{R}'}(\omega) &= \int_V d\mathbf{r} \int_V d\mathbf{r}' \phi^*_{i\mathbf{R}}(\mathbf{r})\phi_{i\mathbf{R}}(\mathbf{r}) W^{\mathrm{el}}(\mathbf{r},\mathbf{r}',\omega)\phi^*_{j\mathbf{R}'}(\mathbf{r}')\phi_{j\mathbf{R}'}(\mathbf{r}') \\ &\quad + \int_V d\mathbf{r} \int_V d\mathbf{r}' \phi^*_{i\mathbf{R}}(\mathbf{r})\phi_{i\mathbf{R}}(\mathbf{r}) W^{\mathrm{ph}}(\mathbf{r},\mathbf{r}',\omega)\phi^*_{j\mathbf{R}'}(\mathbf{r}')\phi_{j\mathbf{R}'}(\mathbf{r}'). \end{aligned} \tag{13}$$

The term $U^{\mathrm{el}}_{i\mathbf{R}j\mathbf{R}'}(\omega) = \langle \phi_{i\mathbf{R}}\phi_{j\mathbf{R}'}| W^{\mathrm{el}}(\omega) |\phi_{i\mathbf{R}}\phi_{j\mathbf{R}'}\rangle$ in the second row is the usual (extended) Hubbard term.

The phonon term of the third row is written as $U^{\mathrm{ph}}_{i\mathbf{R}j\mathbf{R}'}(\omega) = \langle \phi_{i\mathbf{R}}\phi_{j\mathbf{R}'}| W^{\mathrm{ph}}(\omega) |\phi_{i\mathbf{R}}\phi_{j\mathbf{R}'}\rangle$, so that overall we can write the total Coulomb term in the compact form $U^{\mathrm{tot}}_{i\mathbf{R}j\mathbf{R}'}(\omega) = U^{\mathrm{el}}_{i\mathbf{R}j\mathbf{R}'}(\omega) + U^{\mathrm{ph}}_{i\mathbf{R}j\mathbf{R}'}(\omega)$. We now evaluate the phonon-mediated Coulomb term $U^{\mathrm{ph}}_{i\mathbf{R}j\mathbf{R}'}(\omega)$. The phonon propagator appearing in Eq. (11) is written as

$$D_{\mathbf{q},\nu}(\omega) = \frac{1}{\omega - \omega_{\mathbf{q},\nu} + i\delta} - \frac{1}{\omega + \omega_{\mathbf{q},\nu} - i\delta}, \tag{14}$$

where $\omega_{\mathbf{q},\nu}$ the phonon frequency. Substituting the definition of the phonon-screened Coulomb interaction of Eq. (11) in the integral for $U^{\mathrm{ph}}_{i\mathbf{R}j\mathbf{R}'}(\omega)$:

$$\begin{aligned} U^{\mathrm{ph}}_{i\mathbf{R}j\mathbf{R}'}(\omega) &= \langle \phi_{i\mathbf{R}}\phi_{j\mathbf{R}'}| W^{\mathrm{ph}}(\omega) |\phi_{i\mathbf{R}}\phi_{j\mathbf{R}'}\rangle \\ &= \sum_{\mathbf{q},\nu} g_{ii\mathbf{q}\nu}(\mathbf{0}) g^*_{jj\mathbf{q}\nu}(\mathbf{R}'-\mathbf{R}) \\ &\quad \times \left[\frac{1}{\omega - \omega_{\mathbf{q},\nu} + i\delta} - \frac{1}{\omega + \omega_{\mathbf{q},\nu} - i\delta}\right]. \end{aligned} \tag{15}$$

A detailed derivation of this expression is given in Appendix A, where it is also generalized to the case of four-center integrals. Here we use the mixed Wannier-Bloch representation of the electron-phonon coupling matrix element:

$$\begin{aligned} g_{mn\mathbf{q}\nu}(\mathbf{R}) &= \langle \phi_{m\mathbf{R}}| g_{\mathbf{q}\nu} |\phi_{n\mathbf{R}}\rangle \\ &= \sum_{n'm'\mathbf{k}} e^{i\mathbf{q}\cdot\mathbf{R}} w^\dagger_{mn'}(\mathbf{k}+\mathbf{q}) g_{n'm'\nu}(\mathbf{k},\mathbf{q}) w_{m'n}(\mathbf{k}), \end{aligned} \tag{16}$$

where w_{mn} are Wannier rotation matrices, and $g_{nm\nu}(\mathbf{k},\mathbf{q})$ the electron-phonon matrix element in the Bloch basis. As outlined in Appendix D, in principle, one should also account for non-local electron-phonon coupling, captured through matrix elements of the form $g_{mn\mathbf{q}\nu}(\mathbf{R},\mathbf{R}') = \langle \phi_{m\mathbf{R}}| g_{\mathbf{q}\nu} |\phi_{n\mathbf{R}'}\rangle$. These terms will couple electron hopping to phonons, and correspond to a Su-Schrieffer-Heeger mechanism [54,55]. Given the localized nature of Wannier functions, integrals of the form $\langle \phi_{m\mathbf{R}}| g_{\mathbf{q}\nu} |\phi_{n\mathbf{R}'}\rangle$ will be small compared to the local couplings $\langle \phi_{m\mathbf{R}}| g_{\mathbf{q}\nu} |\phi_{n\mathbf{R}}\rangle$, and we will ignore nonlocal coupling for the remainder of this manuscript. However, incorporating these terms from first-principles calculations is an interesting future avenue to pursue within downfolding approaches.

By taking the static limit $\omega = 0$ of Eq. (15), and by considering intraband terms ($i = j$), we obtain the simplified expression

$$U^{\mathrm{ph,st}}_{i\mathbf{R}i\mathbf{R}'} = -2\sum_{\mathbf{q}\nu} \frac{g_{ii\mathbf{q}\nu}(\mathbf{0}) g^*_{ii\mathbf{q}\nu}(\mathbf{R}'-\mathbf{R})}{\omega_{\mathbf{q},\nu}}. \tag{17}$$

The superscript "st" will henceforth denote that we take the static limit $\omega = 0$. If additionally we consider on-site terms $\mathbf{R} = \mathbf{R}'$, we get

$$U^{\mathrm{ph,st}}_{i\mathbf{R}i\mathbf{R}} = -2\sum_{\mathbf{q}\nu} \frac{|g_{ii\mathbf{q}\nu}(\mathbf{0})|^2}{\omega_{\mathbf{q},\nu}}. \tag{18}$$

From Eq. (18), it is clear that in the static limit phonons contribute an attractive term to the on-site Coulomb interaction of electrons.

The effect of phonon screening on on-site Coulomb interactions, similar to Eq. (18), has been computed previously for metals and nonpolar semiconductors, where only short-range electron-phonon coupling is present [3,35]. However, such an approach breaks down for polar materials, where long-range electron-phonon coupling emerges. In these cases, the matrix element is typically written as a sum of a short-range and a long-range terms [36,56]:

$$g_{ij\mathbf{q}\nu} = g^{\mathcal{S}}_{ij\mathbf{q}\nu} + g^{\mathcal{L}}_{ij\mathbf{q}\nu}. \tag{19}$$

The reason for separating these two contributions is that the long-range part $g^{\mathcal{L}}$ scales as $1/|\mathbf{q}|$, leading to a divergence at $\mathbf{q} \to \mathbf{0}$. It is therefore subtracted from the total electron-phonon coupling computed within density functional perturbation theory (DFPT) on a coarse grid, in order to perform a Wannier-Fourier interpolation of the well-behaved short-range part onto a fine grid. The long-range contribution is then added post fact, using an analytical expression [56].

Here we follow a similar approach, where the short-range and long-range electron-phonon coupling are treated separately. The long-range coupling $g^{\mathcal{L}}_{ij\mathbf{q}\nu}$ is computed using the *ab initio* expression [36]:

$$\begin{aligned} g^{\mathcal{L}}_{ij\mathbf{q}\nu}(\mathbf{R}) = i\frac{4\pi}{V}\sum_{\kappa}\left(\frac{1}{2NM_\kappa\omega_{\mathbf{q},\nu}}\right)^{1/2} \frac{\mathbf{q}\cdot\mathbf{Z}_\kappa\cdot\mathbf{e}_{\kappa\nu}(\mathbf{q})}{\mathbf{q}\cdot\epsilon_\infty\cdot\mathbf{q}} \\ \times \langle \phi_{i\mathbf{R}}(\mathbf{r})| e^{i\mathbf{q}\cdot\mathbf{r}} |\phi_{j\mathbf{R}}(\mathbf{r})\rangle, \end{aligned} \tag{20}$$

which is the first-principles generalization of the Fröhlich model. Here $\mathbf{q}$ is the phonon momentum, with the wave vector belonging to a regular grid of N points within the first

Brillouin zone. For an atom κ, M_κ and $\mathbf{Z}_\kappa$ are its mass and Born effective charge tensor respectively, $\mathbf{e}_{\kappa\nu}$ a vibrational eigenvector, and ϵ_∞ the dielectric matrix. In writing expression Eq. (20), we have made the approximation $\mathbf{q}+\mathbf{G} \to \mathbf{q}$, where $\mathbf{G}$ is a reciprocal lattice vector, and also $e^{i\mathbf{q}\cdot\tau_\kappa} \to 1$, where τ_κ the atomic positions. These approximations become accurate in the long-wavelength $\mathbf{q} \to \mathbf{0}$ limit, which dominates the Fröhlich coupling. Moreover, by not considering the contribution of finite $\mathbf{G}$ vectors, we are ignoring local field effects and considering the macroscopic high-frequency dielectric response as defined by ϵ_∞. It is also worth noting that Eq. (20) only allows for longitudinal phonons to couple to the electrons. Transverse phonons have a polarization that is perpendicular to the phonon wave vector $\mathbf{q}$, and, in principle, including the contribution of reciprocal lattice vectors $\mathbf{q}+\mathbf{G}$ could result in a finite contribution by these lattice motions. Nevertheless here we focus on the effect of longitudinal phonons, which is known to generally dominate the long-range coupling to electrons by far [36].

We now insert the electron-phonon vertex of Eq. (20) into Eq. (15) in order to derive the contribution of long-range coupling to the phonon-mediated Hubbard term, denoted as $U^{\mathrm{ph},\mathcal{L}}_{i\mathbf{R}j\mathbf{R}'}(\omega)$. As detailed in Appendix B, this gives us the long-range contribution to the phonon-mediated Coulomb interaction:

$$U^{\mathrm{ph},\mathcal{L}}_{i\mathbf{R}j\mathbf{R}'}(\omega) = \left(\frac{4\pi}{V}\right)^2 \sum_{\mathbf{q}m} \frac{1}{2}\left(\frac{1}{\omega-\omega_{\mathbf{q}m}} - \frac{1}{\omega+\omega_{\mathbf{q}m}}\right) \times \frac{1}{N\omega_{\mathbf{q}m}} \frac{e^{i\mathbf{q}(\mathbf{R}-\mathbf{R}')}}{|\mathbf{q}|^2} \frac{|q_\alpha \mathcal{Z}_{m,\alpha}|^2}{\left(q_\alpha \epsilon^\infty_{\alpha\beta} q_\beta\right)^2}. \tag{21}$$

where we have used the fact that Wannier functions are highly localized around their centers, the index m runs over LO phonons, and the frequency $\omega^2_{\mathbf{q}m}$ refers to the LO phonon. Here we have defined the mode effective charge:

$$\mathbf{q}\cdot\mathcal{Z}_\nu = \sum_\kappa \frac{1}{\sqrt{M_\kappa}} \mathbf{q}\cdot\mathbf{Z}_\kappa\cdot\mathbf{e}_{\kappa\nu}(\mathbf{q}\to\mathbf{0}). \tag{22}$$

The expression of Eq. (21) is amenable to first-principles computation, and its static limit is consistent with the ion part of the total dielectric function that has been derived by Dolgov, Kirzhnits, and Maksymov [57]. This phonon-mediated Coulomb interaction due to the Fröhlich mechanism does not overcome electron-electron repulsion in the static limit $\omega = 0$ [49,57]. Negative values of the total static dielectric function are, in principle, permissible and consistent with a stable dielectric at $\mathbf{q} \neq \mathbf{0}$ [57], but the Fröhlich interaction alone does not give rise to such an effect.

The expression of Eq. (21) may be simplified significantly for isotropic, or mildly anisotropic systems, as we demonstrate in Appendix B. Here we give the final expressions in the static limit, which can be generalized to finite frequencies in a straightforward manner. In every case, the long-range phonon-mediated electron-electron interaction assumes the general form:

$$U^{\mathrm{ph},\mathcal{L}}_{\mathbf{R}\mathbf{R}'}(\omega=0) = -\frac{\gamma^2}{\epsilon|\mathbf{R}-\mathbf{R}'|}, \tag{23}$$

which is always an attractive interaction. For isotropic systems, the dielectric constant ϵ is simply equal to ϵ_∞ and

$$\gamma^2 = \left(\frac{4\pi}{V}\right)\sum_m \frac{|\mathcal{Z}_m|^2}{\epsilon_\infty\,\omega^2_{\mathrm{LO},m}}. \tag{24}$$

For systems with a mild anisotropy, we instead show in Appendix B that $\epsilon = \epsilon^{\mathrm{eff}}_\infty$, with

$$\frac{1}{\epsilon^{\mathrm{eff}}_\infty} \equiv \int \frac{d\Omega}{4\pi}\frac{1}{q_\alpha\epsilon^\infty_{\alpha\beta}q_\beta}, \tag{25}$$

and

$$\gamma^2 = \epsilon^{\mathrm{eff}}_\infty\left(\frac{4\pi}{V}\right)\sum_m \frac{1}{\omega^2_{\mathrm{LO},m}}\int\frac{d\Omega}{4\pi}\frac{|q_\alpha\mathcal{Z}_{m,\alpha}|^2}{\left(q_\alpha\epsilon^\infty_{\alpha\beta}q_\beta\right)^2}, \tag{26}$$

where here we take an orientational average over the unit sphere.

Another interesting limit for the long-range phonon-mediated interaction is obtained for systems where the phonon eigenvectors at $\mathbf{q}\to\mathbf{0}$ are equal to those at $\mathbf{q}=\mathbf{0}$, despite a jump in the frequency value, which is guaranteed by symmetry in some cases. In those cases, the following condition holds [50]:

$$\left(\frac{4\pi}{V}\right)\frac{|q_\alpha\mathcal{Z}_{\nu,\alpha}|^2}{q_\alpha\epsilon^\infty_{\alpha\beta}q_\beta} = \omega^2_{\mathrm{LO},\nu} - \omega^2_{\mathrm{TO},\nu}, \tag{27}$$

which for the isotropic case leads to the following simple expression for the value of γ^2:

$$\gamma^2 = \sum_m \frac{\omega^2_{\mathrm{LO},m}-\omega^2_{\mathrm{TO},m}}{\omega^2_{\mathrm{LO},m}}, \tag{28}$$

and to the long-range phonon-mediated interaction:

$$U^{\mathrm{ph},\mathcal{L}}_{i\mathbf{R}j\mathbf{R}'}(\omega=0) = -\sum_m\left(\frac{\omega^2_{\mathrm{LO},m}-\omega^2_{\mathrm{TO},m}}{\omega^2_{\mathrm{LO},m}}\right)\frac{1}{\epsilon_\infty|\mathbf{R}-\mathbf{R}'|}. \tag{29}$$

We emphasize here that using this simpler expression of Eq. (28) requires one to check the validity of the condition $\mathbf{e}(\mathbf{q}\to\mathbf{0}) = \mathbf{e}(\mathbf{q}=\mathbf{0})$ on a material-by-material basis. While we will not use Eq. (28) to obtain our computational results for the long-range interaction in the main part of our article, we discuss its validity in Appendix C for MgO and GeTe, where it is demonstrated that it holds to good accuracy for these systems.

Moreover, let us consider the long-range phonon-mediated interaction under the assumptions in which the *ab initio* long-range vertex of Eq. (20) reduces to the standard Fröhlich electron-phonon matrix element [58]:

$$g^{\mathrm{Fr}}_{ij\mathbf{q}}(\mathbf{R}) = \frac{i}{|\mathbf{q}|}\sqrt{\frac{4\pi}{NV}\frac{\omega_{\mathrm{LO}}}{2}\left(\frac{1}{\epsilon_\infty}-\frac{1}{\epsilon_o}\right)} \times \langle\phi_{i\mathbf{R}}(\mathbf{r})|\,e^{i\mathbf{q}\cdot\mathbf{r}}\,|\phi_{j\mathbf{R}}(\mathbf{r})\rangle, \tag{30}$$

where ϵ_o the static dielectric constant. The assumptions that reduce Eq. (20) to Eq. (30) are that of Ref. [59] taking the $\mathbf{q}\to 0$ limit for all smoothly-varying quantities, having a band structure identical to that of the electron gas model, the permittivity being isotropic, and having coupling between electrons and a single Einstein LO phonon (hence we have dropped the phonon index ν in Eq. (30)).

Using the Fröhlich vertex of Eq. (30) in Eq. (15) yields

$$U^{\mathrm{ph,Fr},\mathcal{L}}_{i\mathbf{R}j\mathbf{R}'}(\omega)=\frac{\omega_{\mathrm{LO}}}{2}\left(\frac{1}{\omega-\omega_{\mathrm{LO}}}-\frac{1}{\omega+\omega_{\mathrm{LO}}}\right)\times\left(\frac{1}{\epsilon_\infty}-\frac{1}{\epsilon_o}\right)\frac{1}{|\mathbf{R}-\mathbf{R}'|},\tag{31}$$

which in the static limit gives the simple form

$$U^{\mathrm{ph,st,Fr},\mathcal{L}}_{i\mathbf{R}j\mathbf{R}'}=-\left(\frac{1}{\epsilon_\infty}-\frac{1}{\epsilon_o}\right)\frac{1}{|\mathbf{R}-\mathbf{R}'|},\tag{32}$$

which is an attractive screened electron-electron interaction, with both the high- and the low-frequency dielectric constants determining the amount of screening. For $\epsilon_o\to\infty$, the phonon-mediated attraction approaches the value $-1/(\epsilon_\infty|\mathbf{R}-\mathbf{R}'|)$, perfectly canceling the screened electron-electron repulsion, but unable to result in net attraction, consistent with the single-phonon limit of a dielectric discussed in Ref. [57].

IV. CONNECTION TO A LANG-FIRSOV TRANSFORMATION PICTURE

We now connect our results of the previous Sec. III to those obtained within a popular approach within polaron physics, which is taking a Lang-Firsov transformation of a coupled electron-phonon Hamiltonian [51]. This will allow us to develop a better intuition of the underlying assumptions to arrive at the result of Eq. (15). Here we will present the key steps of the derivation, which is given in greater detail in Appendix D.

Consider the coupled electron-phonon Hamiltonian

$$\begin{aligned}H_{\mathrm{pol}}&=\sum_\sigma\sum_{i\mathbf{R},j\mathbf{R}'}t_{i\mathbf{R},j\mathbf{R}'}a^{\sigma\dagger}_{i\mathbf{R}}a^\sigma_{j\mathbf{R}'}\\&+\frac{1}{2}\sum_{\sigma\rho}\sum_{i\mathbf{R},j\mathbf{R}'}U_{i\mathbf{R},j\mathbf{R}'}a^{\sigma\dagger}_{i\mathbf{R}}a^{\rho\dagger}_{j\mathbf{R}'}a^\rho_{j\mathbf{R}'}a^\sigma_{i\mathbf{R}}\\&+\sum_{\mathbf{q}\nu}\omega_{\mathbf{q}\nu}b^\dagger_{\mathbf{q}\nu}b_{\mathbf{q}\nu}+\sum_\sigma\sum_{ij\mathbf{R}\mathbf{q}\nu}g_{ij\mathbf{q}\nu}(\mathbf{R})(b_{\mathbf{q}\nu}+b^\dagger_{-\mathbf{q}\nu})\\&\times a^{\sigma\dagger}_{i\mathbf{R}}a^\sigma_{j\mathbf{R}'},\end{aligned}\tag{33}$$

where the operators $a^{\sigma\dagger}_{i\mathbf{R}}$ ($a^\sigma_{i\mathbf{R}}$) create (destroy) an electron of spin σ in band i and on lattice site $\mathbf{R}$, and $b^\dagger_{\mathbf{q}\nu}$ ($b_{\mathbf{q}\nu}$) creates (destroys) a single phonon at branch ν with momentum $\mathbf{q}$. Let us now perform a Lang-Firsov transformation of the Hamiltonian of Eq. (33). We define

$$S=\sum_\sigma\sum_{i\mathbf{R}\mathbf{q}\nu}a^{\sigma\dagger}_{i\mathbf{R}}a^\sigma_{i\mathbf{R}}\frac{g_{ii\mathbf{q}\nu}(\mathbf{R})}{\omega_{\mathbf{q}\nu}}(b^\dagger_{\mathbf{q}\nu}-b_{-\mathbf{q}\nu})\tag{34}$$

and perform the polaron transformation $\tilde{H}_{\mathrm{pol}}=e^S H_{\mathrm{pol}}e^{-S}$ to eliminate the electron-phonon coupling term. Without relying on any approximation, this leads to the renormalized two-body interaction

$$\tilde{U}_{i\mathbf{R},j\mathbf{R}'}=U_{i\mathbf{R},j\mathbf{R}'}-2\sum_{\mathbf{q}\nu}\frac{g_{ii\mathbf{q}\nu}(\mathbf{R})g^*_{jj\mathbf{q}\nu}(\mathbf{R}')}{\omega_{\mathbf{q}\nu}}.\tag{35}$$

Considering the Bloch periodicity $\tilde{U}_{i\mathbf{R},j\mathbf{R}'}=\tilde{U}_{i\mathbf{0},j\mathbf{R}'-\mathbf{R}}$, this suggests that

$$\tilde{U}_{i\mathbf{R},j\mathbf{R}'}(\omega)=U_{i\mathbf{R},j\mathbf{R}'}(\omega)+U^{\mathrm{ph,st}}_{i\mathbf{R},j\mathbf{R}'},\tag{36}$$

with $U^{\mathrm{ph,st}}_{i\mathbf{R},j\mathbf{R}'}$ the static limit of the phonon-mediated electron-electron interaction, derived in Eq. (17).

Additionally, if we assume the phonon degrees of freedom to be in thermal equilibrium, and trace them out within a weak-coupling approximation, we can replace the phonon operators with their expectation values, in a mean-field fashion. Within its regime of validity, this approximation yields an effective electronic Hamiltonian in the presence of phonons at temperature T:

$$\begin{aligned}H^{\mathrm{el}}_{\mathrm{eff}}&=\sum_\sigma\sum_{i\mathbf{R},j\mathbf{R}'}\tilde{t}_{i\mathbf{R},j\mathbf{R}'}a^{\sigma\dagger}_{i\mathbf{R}}a^\sigma_{j\mathbf{R}'}\\&+\frac{1}{2}\sum_{\sigma\rho}\sum_{i\mathbf{R},j\mathbf{R}'}\tilde{U}_{i\mathbf{R},j\mathbf{R}'}a^{\sigma\dagger}_{i\mathbf{R}}a^{\rho\dagger}_{j\mathbf{R}'}a^\rho_{j\mathbf{R}'}a^\sigma_{i\mathbf{R}},\end{aligned}\tag{37}$$

where we have ignored constant shifts to the electronic energy. Here the modulated off-site interaction is

$$\begin{aligned}\tilde{t}_{i\mathbf{R},j\mathbf{R}'}(T)&=t_{i\mathbf{R},j\mathbf{R}'}\\&\times\exp\left[-\sum_{\mathbf{q}\nu}\frac{|g_{jj\mathbf{q}\nu}(\mathbf{R}')-g_{ii\mathbf{q}\nu}(\mathbf{R})|^2}{\omega^2_{\mathbf{q}\nu}}\right.\\&\left.\times\left(N_{\mathbf{q}\nu}(T)+\frac{1}{2}\right)\right],\end{aligned}\tag{38}$$

where $N_{\mathbf{q}\nu}(T)$ the Bose-Einstein distribution. The on-site energies are renormalized as

$$\tilde{t}_{i\mathbf{R},i\mathbf{R}}=t_{i\mathbf{R},i\mathbf{R}}-\sum_{\mathbf{q}\nu}\frac{|g_{ii\mathbf{q}\nu}(\mathbf{0})|^2}{\omega_{\mathbf{q}\nu}}.\tag{39}$$

It should again be emphasized that the above result for the temperature-dependent modulation of the hopping term relies on the weak-coupling approximation, which is violated in systems with strong electron-phonon interactions, such as MgO.

Let us pause to consider what has been achieved at this point. Eq. (37) is a generalized Hubbard model, including only electronic terms, with the hopping and Coulomb integrals renormalized by the magnitude of the electron-phonon interactions. One can solve this Hamiltonian in exactly the same manner as the original Hamiltonian (2), with the only difference that the parameters entering it are renormalized. Moreover the correction to the two-body Coulomb term due to phonons is found to be identical to the static phonon-mediated correction of Eq. (17). Therefore, starting from the coupled electron-phonon Hamiltonian of Eq. (33), performing a Lang-Firsov transformation and tracing out phonon degrees of freedom, yields the static limit of including phonon screening in the Coulomb integral of Eq. (4).

It is interesting to note at this point some characteristics of the temperature dependence of the effective electronic Hamiltonian of Eq. (37). The phonon-induced renormalization of the hopping terms, as described by Eq. (38), is temperature-dependent, with the hopping integrals reduced with increasing temperature, indicative of a flattening of the electronic bands, and real-space localization of electronic states, in agreement with previous derivations [60,61]. However, the correction to the Coulomb term describes virtual phonon processes and hence is temperature-independent. For the remainder of this paper we will focus on the renormalization of the Coulomb interactions.

V. COMPUTATIONAL IMPLEMENTATION

We now return to Eq. (15) for the general frequency-dependent phonon correction to the Coulomb interactions, and its computational implementation. Moreover, below we discuss the practical calculation of the long-range part of the electron-phonon interaction, which is treated separately in order to allow for the Wannier-Fourier interpolation of the short-range coupling $g^{\mathcal{S}}$.

A notable characteristic of Eq. (15) is that the electron-phonon matrix elements appear in a mixed Wannier-Bloch basis, for the electronic and phonon degrees of freedom, respectively. Within our formalism, the lattice vectors $\mathbf{R}$ indicate the centers of Wannier functions, with $\mathbf{R} = \mathbf{R}'$ representing an on-site term and $\mathbf{R} \neq \mathbf{R}'$ off-site terms, the range of which is determined by the distance of the Wannier centers. The effect of phonons on each of the lattice terms $U^{\mathrm{ph}}_{i\mathbf{R}j\mathbf{R}'}(\omega)$ is determined by summing over the phonon momentum grid $\mathbf{q}$, and the sum needs to be converged by using a fine mesh. However, unlike most studies that evaluate electron-phonon self-energies from first principles [52,62,63], here we do not need to also evaluate the electronic degrees of freedom on a dense grid. There is therefore only a need to perform Wannier-Fourier interpolation for $\mathbf{q}$-vectors (and not $\mathbf{k}$ vectors). As discussed previously, we only perform Wannier-Fourier interpolation for the short-range electron-phonon matrix element $g^{\mathcal{S}}$, in order to avoid the singular behavior of the long-range term, which we add analytically, directly on a fine $\mathbf{q}$-grid.

Similarly to using constrained RPA rather than regular RPA to compute the polarizability of Eq. (9), as a means of excluding the screening of the states of the active space within which we derive the Coulomb interactions, here we employ constrained density functional perturbation theory (cDFPT) [31] rather than usual DFPT, to obtain the short-range electron-phonon matrix elements $g^{\mathcal{S}}$ entering the phonon-renormalized Coulomb terms of Eq. (15). We use the modified version of Quantum Espresso [64] of Ref. [34] to perform cDFPT calculations on a coarse $\mathbf{q}$ grid, and we determine the Wannier representation of our systems using Wannier90 [65]. Within the cDFPT calculations, we obtain phonon frequencies and electron-phonon matrix elements of states within an active space, which is defined on a case-by-case basis for studied materials. We perform Wannier-Fourier interpolation of short-range electron-phonon coupling matrix elements on a fine $\mathbf{q}$ grid within the EPW code [66], and we extract $g^{\mathcal{S}}_{ij\mathbf{q}\nu}(\mathbf{R})$ using a modified version of the code. Therefore we obtain converged values for the short-range contribution to the phonon renormalization of the Hubbard term $U^{\mathrm{ph},\mathcal{S}}_{i\mathbf{R}j\mathbf{R}'}(\omega) = \sum_{\mathbf{q},\nu} g^{\mathcal{S}*}_{ij\mathbf{q}\nu}(\mathbf{0}) g^{\mathcal{S}}_{ij\mathbf{q}\nu}(\mathbf{R}'-\mathbf{R})[\frac{1}{\omega-\omega_{\mathbf{q},\nu}+i\delta} - \frac{1}{\omega+\omega_{\mathbf{q},\nu}-i\delta}]$. We obtain the electronic Coulomb interactions within the same active space using cRPA, and specifically Eqs. (4) and (9) as implemented in RESPACK [67] in each case. We use Eq. (23) to compute the long-range contribution $U^{\mathrm{ph},\mathcal{L}}_{i\mathbf{R}j\mathbf{R}'}(\omega)$, in its isotropic or anisotropic manifestation depending on the studied material, and yielding the overall result $U^{\mathrm{ph}}_{i\mathbf{R}j\mathbf{R}'}(\omega) = U^{\mathrm{ph},\mathcal{S}}_{i\mathbf{R}j\mathbf{R}'}(\omega) + U^{\mathrm{ph},\mathcal{L}}_{i\mathbf{R}j\mathbf{R}'}(\omega)$.

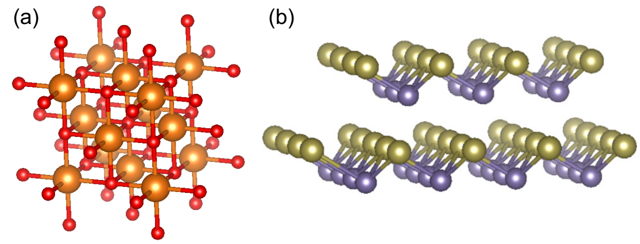

FIG. 2. Structures of MgO (a) and GeTe (b). Mg atoms are shown in orange, O in red, Ge in purple, and Te in gold. The structures are visualized in VESTA [72].

VI. STUDIED STRUCTURES AND COMPUTATIONAL DETAILS

Below we outline the details of our calculations for MgO and GeTe. We have chosen MgO since it is a prototypical bulk insulator with strong long-range electron-phonon coupling, hence providing an excellent material to demonstrate the impact of our formalism and of polar contributions to its electron-electron interactions. Moreover, short-range electron-phonon interactions are known to also modify the electronic structure by a non-negligible amount [68], making the interplay of these effects at different length scales an interesting one to explore. Semiconducting GeTe on the other hand is known to exhibit superconductivity and strong electron-phonon interactions [69,70], we were therefore interested in understanding whether our framework could provide an explanation for the formation of Cooper pairs in this material. The structural details of MgO and GeTe are given in Table I, and the studied structures are also visualized in Fig. 2. The structures were taken from the Materials Project database [71]. MgO forms a cubic rocksalt structure GeTe is studied in its low-temperature trigonal phase, which consists of GeTe bilayers along the c axis.

We employ QUANTUM ESPRESSO [64] for all DFT and DFPT calculations, Wannier90 [65] in order to generate the Wannier representation of the active space of interest, as discussed in Sec. VII, and EPW [66] in order to perform Wannier-Fourier interpolation of electron-phonon matrix elements. We employ scalar-relativistic optimized norm-conserving Vanderbilt pseudopotentials (ONCV) [73] with standard accuracy, taken from PSEUDO DOJO [74]. Specifically, these include three valence electrons for Mg, two valence electrons for O, three valence electrons for Ge, and three valence electrons for Te.

For MgO, we work within the generalized gradient approximation (GGA) of DFT as formulated by Perdew, Burke, and Ernzerhof (PBE) [75]. We use a plane wave cutoff of 80 Ry. As a starting point for downfolding calculations of the electronic structure, we compute the electronic density on a $6 \times 6 \times 6$ Γ-centered $\mathbf{k}$ grid, and we include 300 bands in the cRPA calculations, using a cutoff of 7 Ry, and having excluded the three highest-lying valence bands as discussed in Sec. VII. For cDFPT calculations, we use an electronic

TABLE I. Studied materials, their structure, primitive lattice constants, angles, and volumes, space group, and identifier in the Materials Project database [71]. For GeTe, we performed geometry optimization for the atomic positions and lattice parameters, using DFT within the LDA, which has been discussed to yield accurate structural properties for this system [76].

Material	Crystal System	Structure	a (Å)	α	V (Å^3)	Space Group	Identifier
MgO	Cubic	Halite, Rock Salt	2.97	60.0°	26.198	$Fm\bar{3}m$	mp-1265
GeTe	Trigonal	Halite, Rock Salt	4.19	59.08°	50.93	$R\bar{3}m$	mp-938

density computed on a $6 \times 6 \times 6$ half-shifted **k** grid, and we obtain the phonons on a $6 \times 6 \times 6$ grid of **q** points. We interpolate the phonon frequencies and electron-phonon matrix elements on a $20 \times 20 \times 20$ **q** grid, which we find is sufficient to converge the values of the short-range phonon-mediated contribution to the Coulomb interactions within the valence bands, i.e., $U^{\mathrm{ph},\mathcal{S}}_{i\mathbf{R}j\mathbf{R}'}(\omega)$. When it comes to computing the long-range phonon-mediated Coulomb term $U^{\mathrm{ph},\mathcal{L}}_{i\mathbf{R}j\mathbf{R}'}(\omega)$, we use the isotropic limit $-\gamma^2/(\epsilon_\infty r)$, with γ given by Eq. (24), given the isotropy of the crystal and its dielectric properties.

For GeTe, we work within the local density approximation (LDA), which is known to lead to accurate phonon and dielectric properties for this system [76]. We optimize the atomic positions and lattice parameter of the system prior to any other calculations, using a plane wave cutoff of 100 Ry, on a $12 \times 12 \times 12$ half-shifted **k** grid. The resulting structural parameters of Table I are in close agreement to previously reported theoretical values [76]. Beyond the geometry optimization, we use a plane wave cutoff of 100 Ry across all DFT calculations on this system. As a starting point for downfolding calculations of the electronic structure, we compute the electronic density on a $6 \times 6 \times 6$ Γ-centered **k** grid, and we include 700 bands in the cRPA calculations, using a cutoff of 7 Ry, and having excluded the three highest-lying valence bands as discussed in Sec. VII. For cDFPT calculations, we use an electronic density computed on a $12 \times 12 \times 12$ half-shifted **k** grid, and we obtain the phonons on a $12 \times 12 \times 12$ grid of **q** points. We compute the short-range term $U^{\mathrm{ph},\mathcal{S}}_{i\mathbf{R}j\mathbf{R}'}(\omega)$ on the same $12 \times 12 \times 12$ grid, we therefore do not need to perform any interpolation of phonon frequencies and electron-phonon matrix elements in this case. Given the layered character of this material, we utilize the anisotropic definition of Eq. (26) for γ and obtain $U^{\mathrm{ph},\mathcal{L}}_{i\mathbf{R}j\mathbf{R}'} = -\gamma^2/(\epsilon_{\mathrm{eff}} r)$.

VII. COMPUTATIONAL RESULTS

Below we outline our computational results for *ab initio* downfolding of the electronic structure of MgO and GeTe, and we include the effects of phonon screening.

A. MgO

We begin our analysis of MgO with a discussion of its electronic band structure, visualized in Fig. 3(a). We focus on computing the electronic interactions of carriers within the subspace of the three highest-lying valence bands, for which our Wannier-interpolated band structure is visualized in red in Fig. 3(a). These bands are dominated by oxygen p orbitals, and the Wannier functions are centered on O atoms, with a distance between neighboring sites that is equal to the primitive lattice constant of 2.97 Å. Below we focus on computing the phonon-induced renormalization of the Coulomb interactions within this subspace using *ab initio* downfolding and our extension of it to account for phonon screening. The phonon dispersion of MgO is visualized in Fig. 3(b). The unit cell of this system consists of two atoms, and there are therefore six phonons, with a single longitudinal optical (LO) mode with a Γ frequency of 86 meV, and two transverse optical (TO) phonons with a Γ frequency of 49 meV. We also compute the Born effective charges associated with the Mg and O atoms, reported in Table II, which are very close to the oxidation numbers of these elements, indicating the strong ionic character of the bonding. In Table III, we give the values for the

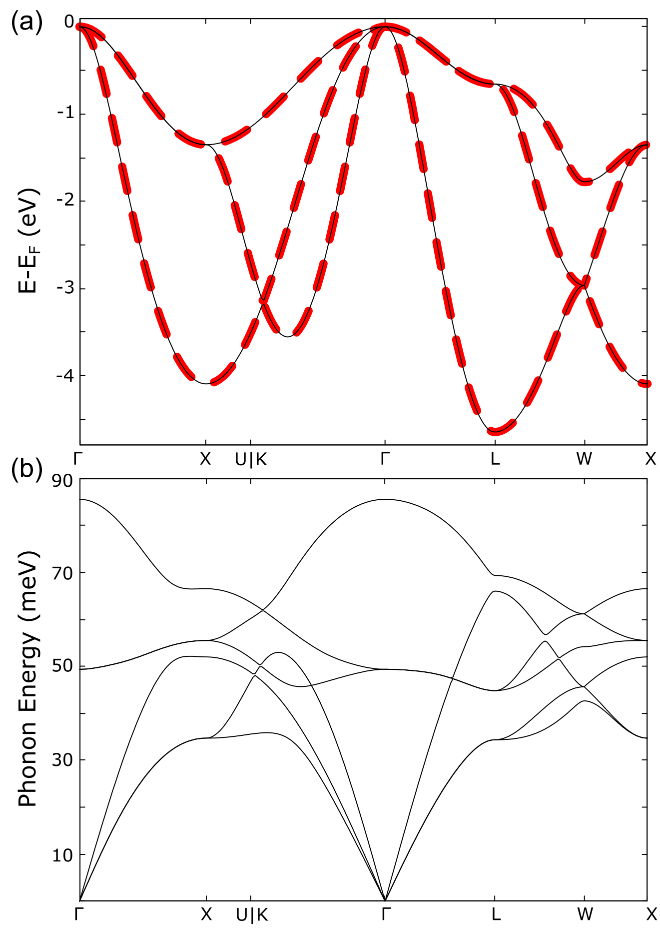

FIG. 3. Electronic band structure (a) and phonon dispersion (b) of MgO computed at the DFT-GGA level of theory as discussed in the main text. The red dashed lines in (a) indicate our Wannier-interpolated bands for the three highest valence bands, which constitute our active space for *ab initio* downfolding.

TABLE II. Born effective charges of MgO.

Atom	Z^*
Mg	1.989
O	−1.985

static intraband (band-averaged) on-site Hubbard term $U^{\mathrm{el}} = \frac{1}{3}\sum_i U^{\mathrm{el}}_{i\mathbf{R}i\mathbf{R}}(\omega=0)$ of the MgO valence bands within the active space, where we have used the expression of Eq. (4). We also report the nearest-neighbor (band-averaged) Coulomb repulsion $V^{\mathrm{el}} = \frac{1}{3}\sum_i U^{\mathrm{el}}_{i\mathbf{R}i\mathbf{R}'}(\omega=0)$, with the lattice vectors $\mathbf{R}, \mathbf{R}'$ indicating nearest-neighbor positions in this case. Here "nearest neighbor" refers to the distance between Wannier function centers, which for MgO coincide with the positions of O atoms. We find a $U^{\mathrm{el}} = 6.826$ eV on-site repulsion of the electrons in the valence bands, and a $V^{\mathrm{el}} = 1.393$ eV nearest-neighbor repulsion. While here we have focused on the intraband electron-electron repulsion, the interband terms are also found to be of comparable magnitude. Moreover, we report in Table III the high-frequency and static dielectric constants as obtained from DFPT.

We now consider the phonon-induced renormalization of the intraband terms $U^{\mathrm{el}}, V^{\mathrm{el}}$, in the static limit. The short-range electron-phonon coupling contribution $U^{\mathrm{ph,st}}, V^{\mathrm{ph,st},\mathcal{S}}$ to the on-site and nearest-neighbor electron-electron interaction respectively is computed using Eq. (17). As we report in Table III, we find a renormalization of the on-site term of $U^{\mathrm{ph,st}} = -2.720$ eV, bringing the overall on-site interaction to $U^{\mathrm{tot}}(\omega=0) = U + U^{\mathrm{ph,st}} = 4.106$ eV, i.e., phonons reduce the repulsive interaction by 39.8% compared to the case where their effect is ignored. Short-range electron-phonon coupling also leads to a weak attraction $V^{\mathrm{ph,st},\mathcal{S}} = -11$ meV between nearest neighbors. Moreover, we find for both the on-site and nearest-neighbor terms that the correction to the interband electron-electron interaction due to short-range electron-phonon coupling is of comparable magnitude to the intra-band values of these quantities.

Importantly, we find that long-range electron-phonon coupling induces a large attraction between electrons in MgO, particularly when these are on neighboring sites (the on-site correction $\mathbf{R} = \mathbf{R}'$ is ill-defined for the long-range contribution). Given the isotropic character of MgO, we compute γ^2 using Eq. (24), and obtain the phonon-induced attraction in the static limit as $-\gamma^2/(\epsilon_\infty r)$. We find an attraction $V^{\mathrm{ph,st},\mathcal{L}} = -1.005$ eV between electrons on neighboring sites in MgO, as summarized in Table III together with our computed value for γ^2. This strong effect is *in addition* to the weak effect of short-range electron-phonon coupling on nearest neighbor interactions, as incorporated within the established cDFPT approach [3]. As we saw, for MgO, this short-range contribution leads to an attraction of $V^{\mathrm{ph,st},\mathcal{S}} = -11$ meV between neighboring electrons. It therefore becomes clear that within downfolded representations of polar materials, long-range electron-phonon coupling can dominate, and including it is imperative for the derived model Hamiltonians to faithfully represent the low-energy physics.

We now turn to the frequency dependence of the correction $U^{\mathrm{ph}}(\omega)$ to the on-site Hubbard term, following Eq. (15). In Fig. 4, we visualize $U^{\mathrm{tot}}(\omega) = U^{\mathrm{el}}(\omega) + U^{\mathrm{ph}}(\omega)$ over a range of frequencies that covers the entire phonon spectrum of the material. Within this range, the frequency dependence of the electronic term is negligible, and oscillations are almost entirely due to the phonon term. To improve visibility, which can be obscured by strong oscillations in the vicinity of poles, we have applied a Gaussian smoothing filter to reduce noise and emphasize the overall trend. It is evident from Fig. 4 that the Hubbard term exhibits a strong frequency dependence, particularly around phonon energies (red dashed lines), where it may even assume negative values depending on how finely we sample on the frequency grid. As expected, at frequencies above the highest phonon energy of the system, the Coulomb term approaches the purely electronic value U^{el} (blue dashed line). The importance of the frequency dependence for obtaining quantitatively accurate eigenstates of the downfolded Hamiltonian has been discussed previously in the context of excited state calculations [39].

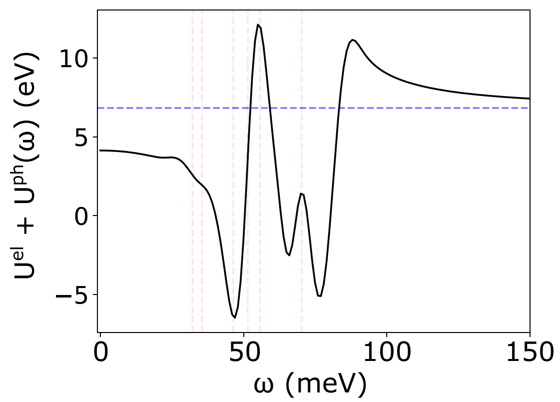

FIG. 4. Frequency-dependence of the total on-site Hubbard term for the highest-lying valence band of MgO. The red vertical lines indicate the average phonon frequencies on the $20 \times 20 \times 20$ **q** grid where U^{ph} is computed, while the blue horizontal line marks the value of the electronic Hubbard term of 6.826 eV for this band, in the $\omega = 0$ limit.

We now analyze how different phonons contribute to the overall renormalization of the electronic interactions. We visualize in Fig. 5 the phonon-resolved values of the on-site correction $U^{\mathrm{ph,st}}$. We see that the most important contribution

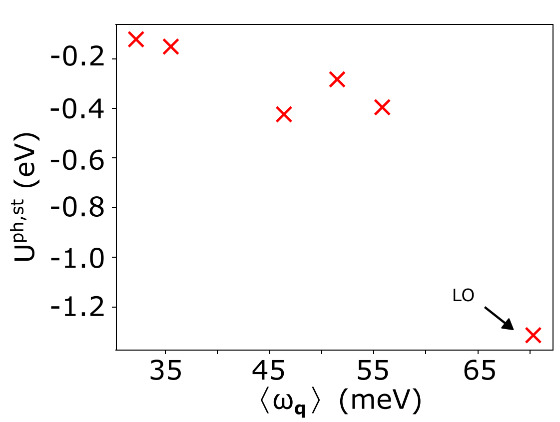

FIG. 5. Contributions of individual phonon modes to the renormalization of the on-site Hubbard term of MgO.

TABLE III. Numerical results for MgO: High-frequency and static dielectric constants, γ^2 following Eq. (24), static on-site and nearest neighbor Coulomb repulsion, static on-site and nearest-neighbor phonon-induced attraction due to short-range electron-phonon coupling, and static nearest-neighbor phonon-induced attraction due to long-range electron-phonon coupling.

ϵ_∞	ϵ_o	γ^2	U^{el} (eV)	V^{el} (eV)	$U^{\mathrm{ph,st}}$ (eV)	$V^{\mathrm{ph,st},\mathcal{S}}$ (eV)	$V^{\mathrm{ph,st},\mathcal{L}}$ (eV)
3.22	9.67	0.660	6.826	1.393	−2.720	−0.011	−1.005

arises from the LO phonon, but there are also significant contributions from the TO and acoustic phonons of MgO. Unlike the long-range electron-phonon interaction, which is dominated by the Fröhlich mechanism where exclusively LO phonons contribute, short-range electron-phonon coupling may be significant also for transverse optical and acoustic phonons, as we observe in Fig. 5. There have been previous reports in the literature for the magnitude of the short-range electron-phonon interaction in materials such as TiO_2 [36], where it was found to be significant, although substantially weaker than the long-range coupling. Indeed, for off-site terms V, the long-range phonon-mediated electronic interaction dominates over the short-range one as seen in Table III. Nevertheless, short-range electron-phonon coupling results in a significant renormalization of the on-site electronic repulsion.

At this point, it is worth emphasizing some of the physical characteristics of the contribution of the short-range electron-phonon interaction to the renormalization of the Coulomb interactions within the valence bands. In Fig. 6, we visualize the on-site phonon-mediated Coulomb interaction $U^{\mathrm{ph,st}}$ in the static limit, due to the LO phonon (panel (a)) and due to one of the TO phonons (panel (b)), as a function of the phonon momentum $|\mathbf{q}|$. Here we have chosen two paths along the Brillouin zone where the effect is significant. We see that short-range electron-phonon coupling can cause an attraction with complex dependence on $|\mathbf{q}|$, unlike the $1/|\mathbf{q}|^2$ dependence due to long-range Fröhlich coupling. This short-range interaction is due to the so-called deformation potential mechanism. As discussed in analytic theories of electron-phonon coupling [77], the matrix elements describing the interaction within this mechanism generally consist of a constant part, as well as octopole and higher-order terms that depend on $\mathbf{q}$, which vanish as $\mathbf{q} \to 0$. The $\mathbf{q}$-independent part of the deformation potential is highly band-dependent and can vanish due to symmetry in several cases, for example for the LO phonons of direct gap semiconductors, and for coupling within conduction bands [78]. Indeed we see that for MgO, the short-range contribution to the phonon-mediated Coulomb term vanishes for $\mathbf{q} \to 0$ (Fig. 6(a)).

B. GeTe

Next we consider the effect of phonon screening on the electron-electron interactions of semiconducting GeTe. The electronic band structure and phonon dispersion of this system are visualized in Fig. 7. We see that there exists a manifold of three fairly isolated valence bands near the Fermi level, and these form the active space within which we compute the electron-electron interactions. Approximately 68% of the wave function amplitude for these bands corresponds to contributions from Te p orbitals, with the remaining 32% coming from Ge p orbitals. As a result, the resulting Wannier functions have strong p-orbital character, and are not perfectly centered on either atom within the unit cell, having a nearest neighbor distance of 4.19 Å, i.e., equal to the primitive lattice constant. Given the proximity of the conduction bands to the valence band manifold within the DFT-LDA level of theory, we repeated the analysis presented below, this time including the three lowest conduction states in the active space. At least for the phonon-mediated electron-electron interactions within the top valence band, we found that this leads to only minor differences in the results.

The trigonal phase of GeTe has two atoms in its primitive cell, there are therefore six phonons, with a single LO mode, highlighted in Fig. 7(b). The layered structure of GeTe makes

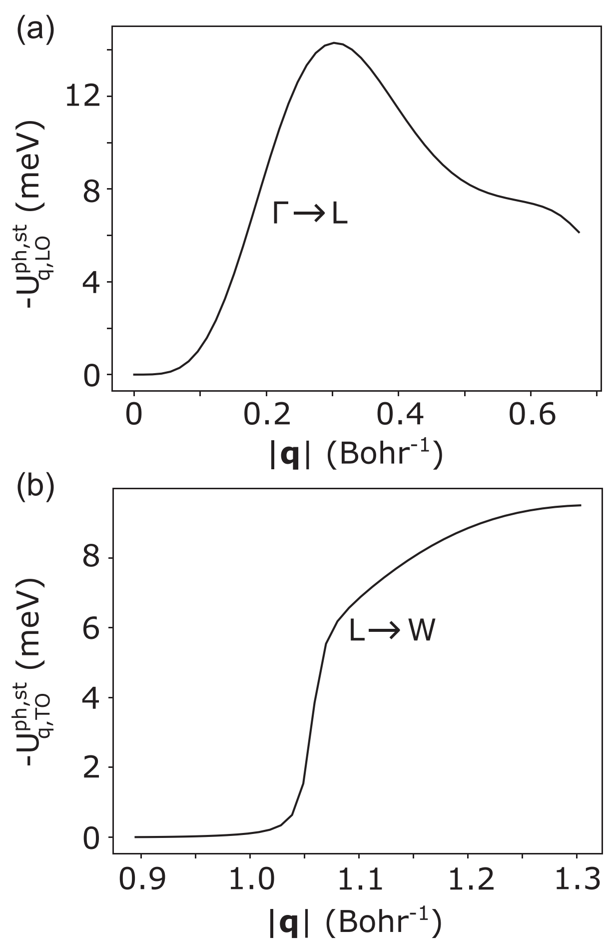

FIG. 6. Dependence of the short-range phonon-induced correction of the on-site Coulomb interaction on the phonon momentum, in the static limit. This is visualized for the LO phonon of MgO, along the $\Gamma \to L$ path in reciprocal space (a), and for a TO phonon along the $L \to W$ path (b).

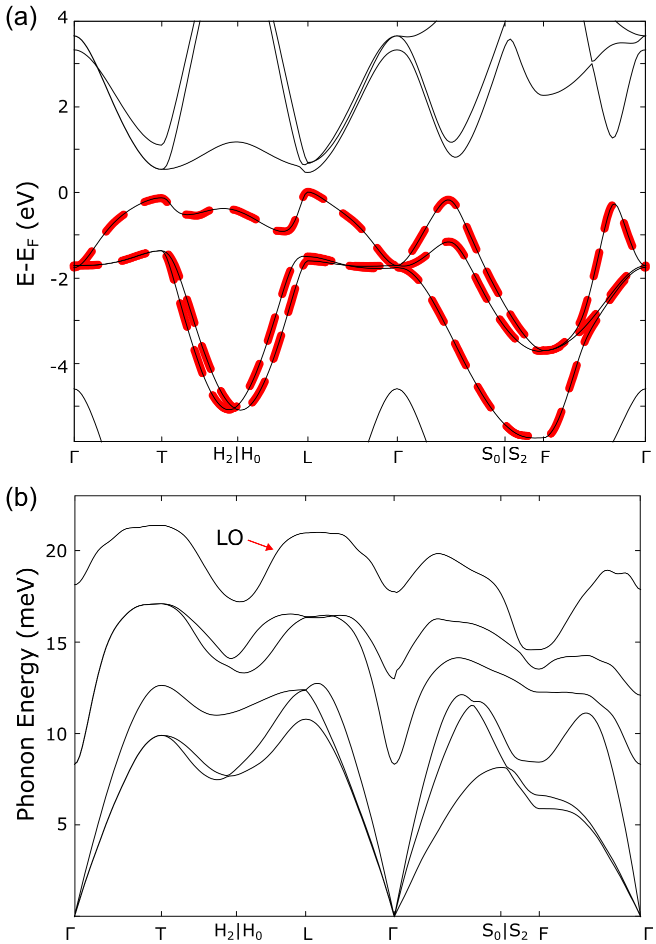

FIG. 7. Electronic band structure (a) and phonon dispersion (b) of GeTe computed at the DFT-LDA level of theory as discussed in the main text. The red dashed lines in (a) indicate our Wannier-interpolated bands for the highest three valence bands, which constitute our active space for *ab initio* downfolding.

this system anisotropic, therefore, the precise energy of the LO phonon depends on the direction of $\mathbf{q}$, as $\mathbf{q} \to \mathbf{0}$. This anisotropy is reflected in the values of the Born effective charges associated with the Ge and Te atoms, as reported in Table IV, which assume different in-plane and out-of-plane values, and similarly for the high-frequency and static dielectric constants reported in Table V. Given the anisotropy of the system, the long-range phonon-mediated attraction is obtained as $-\gamma^2/(\epsilon_{\rm eff} r)$, where $\epsilon_{\rm eff}$ is the spherical average of the dielectric tensor following Eq. (25), and similarly γ^2 is obtained from Eq. (26), where an orientational average over the unit sphere is taken. Table V reports the values for $\epsilon_{\rm eff}$ and γ^2 that we obtain here. The magnitude of the on-site and nearest-neighbor electron-electron repulsion is given in Table V, as is the phonon-induced renormalization of these. Here we give the intraband values for the top valence band within the active space, however, similar to the case of MgO, the interband phonon-mediated interactions are found to be of comparable magnitude. Despite the anisotropic character of the system, the values of these quantities do not significantly change depending on the spatial direction, we therefore only give the values for the in-plane interactions for brevity. The

TABLE IV. Born effective charges of GeTe.

Atom	$Z^*_\parallel$	$Z^*_\perp$
Ge	7.139	5.081
Te	−7.019	−4.995

first striking observation from the results of Table V is that the on-site Coulomb repulsion $U^{\rm el} = 1.102$ eV is strongly renormalized by phonons, leading to a total interaction of $U^{\rm tot} = U^{\rm el} + U^{\rm ph} = 0.229$ eV in the static limit, i.e., amounting to a 79% reduction of the electronic repulsion due to phonon screening. The second interesting observation is that the total phonon-induced attraction between nearest neighbor sites, due to the combined effects of short-range and long-range electron-phonon coupling, is equal to $V^{\rm ph,st,tot} = V^{\rm ph,st,\mathcal{S}} + V^{\rm ph,st,\mathcal{L}} = -0.166$ eV, which will not only completely screen out the repulsive electron-electron term $V^{\rm el} = 0.118$ eV, but will even result in an overall attractive interaction of $V^{\rm el} + V^{\rm ph,st,tot} = -0.048$ eV in the static limit.

Interestingly, unlike the case of MgO where the nearest-neighbor phonon-induced attractive interaction is almost entirely due to long-range electron-phonon coupling, we see in Table V, that for GeTe the short-range term $V^{\rm ph,st,\mathcal{S}}$ is in fact more negative than the long-range part $V^{\rm ph,st,\mathcal{L}}$. To better understand this result, we plot in Fig. 8 the spatial decay of the static phonon-induced attraction for short-range and long-range electron-phonon coupling. As expected, the short-range part decays rapidly, quickly reducing to a negligible contribution with increasing distance between the lattice sites $|\mathbf{R} - \mathbf{R}'|$. Its most important contributions are found for small distances, primarily for the on-site interaction, where as discussed previously, it induces a 79% reduction of the electronic repulsion. Despite the fast decay of this term with increasing distance, its strong on-site value leads to a still appreciable contribution for nearest neighbors, which is in fact more attractive than that of the generalized Fröhlich vertex. Nevertheless, here too the long-range mechanism of the electron-phonon interaction leads to an appreciable renormalization of the electron-electron interaction, and incorporating it in the downfolded representation of GeTe is important towards achieving predictive accuracy for the physics of this system. Moreover, the Fröhlich term remains finite at large values of $|\mathbf{R} - \mathbf{R}'|$, given its long-range character.

Now let us consider the frequency dependence of the on-site electron-electron interactions, once phonon screening is accounted for, visualized in Fig. 9. We see that already for small values of the electronic frequency and as we are approaching the phonon poles, the on-site Coulomb interaction assumes negative values. Moreover, for larger frequency values in the plotted range, the total electronic interaction $U^{\rm el} + U^{\rm ph}(\omega)$ approaches the static limit of the purely electronic contribution, as expected.

The strong variations of the frequency-dependent interaction strength in Fig. 9 as one approaches the poles corresponding to acoustic and optical phonons suggest that the screening from several modes renormalize the electron-electron interactions strongly. In Fig. 10, we plot the attractive contribution of different phonons in the static limit. Similar

TABLE V. Numerical results for GeTe: High-frequency and static dielectric constants, γ^2 following Eq. (26), static on-site and nearest neighbor Coulomb repulsion, static on-site and nearest-neighbor phonon-induced attraction due to short-range electron-phonon coupling, and static nearest-neighbor phonon-induced attraction due to long-range electron-phonon coupling.

$\epsilon_\infty^\parallel$	$\epsilon_o^\parallel$	$\epsilon_\infty^\perp$	$\epsilon_o^\perp$	$\epsilon_\infty^{\rm eff}$	γ^2	$U^{\rm el}$ (eV)	$V^{\rm el}$ (eV)	$U^{\rm ph,st}$ (eV)	$V^{\rm ph,st,\mathcal{S}}$ (eV)	$V^{\rm ph,st,\mathcal{L}}$ (eV)
61.90	279.33	51.29	93.71	57.91	0.649	1.102	0.118	−0.873	−0.128	−0.038

to MgO, the LO phonon again dominates this short-range contribution to the attractive interaction. However, it is worth noting that acoustic modes also provide a very significant attraction in this case. This is attributed to the strong piezoelectric electron-phonon interaction in GeTe [76], which also manifests as strong phonon screening from acoustic modes in other piezoelectrics, such as CdS [52].

In order to gain more insights into the microscopic mechanism of the phonon-induced electron-electron attraction due to short-range interactions, we plot in Fig. 11 the dependence of $U^{\rm ph,st}$ in the static limit on the phonon momentum $|\mathbf{q}|$, for the LO phonon (panel (a)) and for the dominant acoustic mode (panel (b)). For the LO phonon, we see that $U^{\rm ph}$ is roughly proportional to $|\mathbf{q}|$ and vanishes at Γ, in accordance with a deformation potential mechanism. This channel is particularly strong in GeTe, due to the large values of the Born effective charges in this material (Table IV), which constitute the character of the Ge-Te bond mixed ionic-covalent; a feature which is commonly associated with strong deformation potential [79]. Intuitively, this can be understood as having a significant charge localization on the atoms, making distortions of the atomic configuration particularly impactful on the properties of the electronic wave function. This is similar to the mechanism of electron-phonon coupling in molecular crystals and molecules in vacuum, where strong electronic localization leads to stronger coupling to vibrations associated with local atomic distortions [27,80]. The acoustic phonon on the other hand, does not demonstrate behavior consistent with a deformation potential mechanism as in the case of MgO, with its contribution growing as we approach the Γ point. As already stated previously, this is consistent with the piezoelectric mechanism of the electron-phonon interaction. These terms arise from long-range quadrupole contributions, which are captured within DFPT calculations of the electron-phonon matrix elements [81]. Similar to the dipole terms, the quadrupole terms should be subtracted from the electron-phonon matrix elements prior to Wannier-Fourier interpolation [66,82], in order to avoid irregular behavior, particularly in the $\mathbf{q} \rightarrow \mathbf{0}$ region. However, for GeTe, we do not perform any interpolation of the electron-phonon matrix elements, as outlined in Sec. VI, it is therefore not necessary to subtract the quadrupole terms from our short-range electron-phonon matrix elements computed from DFPT, and hence the piezoelectric phonon-mediated electron-electron interaction in GeTe is captured within our approach.

Our first-principles formalism predicts the emergence of overall attractive nearest-neighbor interactions in the valence bands of GeTe, in the static limit, which arise from the interplay between the Fröhlich, deformation potential, and piezoelectric mechanisms of electron-phonon coupling. Such an attractive nearest neighbor attraction has commonly been connected to the emergence of superconductivity [82–85]. Additionally, the frequency dependence of the on-site Hubbard term due to phonon contributions, visualized in Fig. 9, demonstrates that this term also becomes attractive at relatively low electronic energies, which could be relevant already at relatively low doping levels, and which could

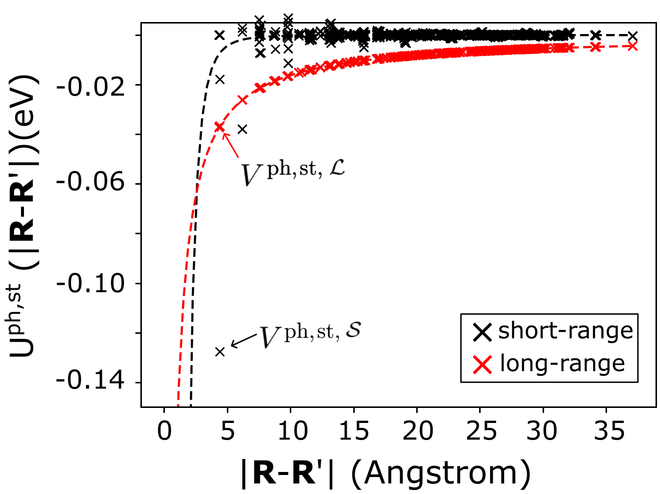

FIG. 8. Spatial decay of the static phonon-induced electron-electron attraction in GeTe, due to short-range and long-range electron-phonon coupling. The dashed lines serve as a guide to the eye.

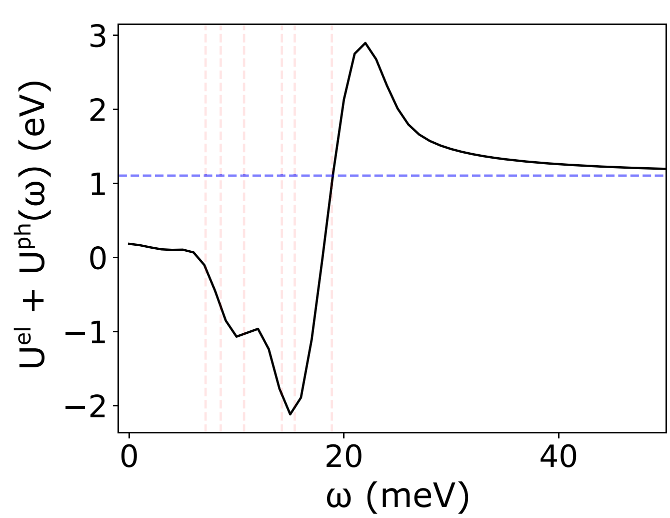

FIG. 9. Frequency dependence of the total on-site Hubbard term for the highest-lying valence band of GeTe. The red vertical lines indicate the average phonon frequencies on the 20 × 20 × 20 **q** grid where $U^{\rm ph}$ is computed, while the blue horizontal line marks the value of the electronic Hubbard term of 1.102 eV for this band, in the $\omega = 0$ limit.

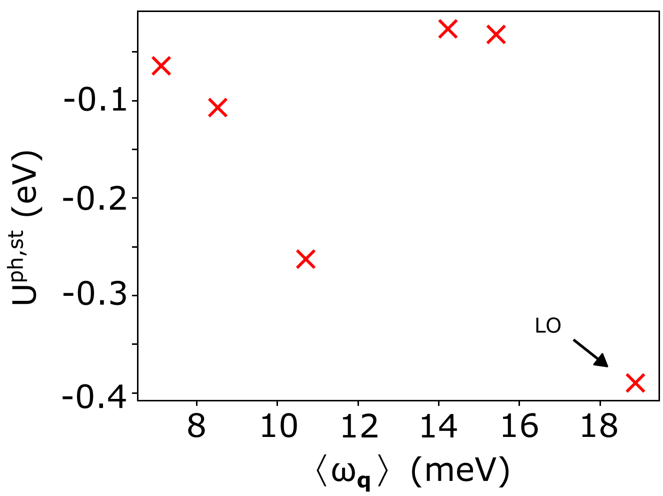

FIG. 10. Contributions of individual phonon modes to the renormalization of the on-site Hubbard term of GeTe.

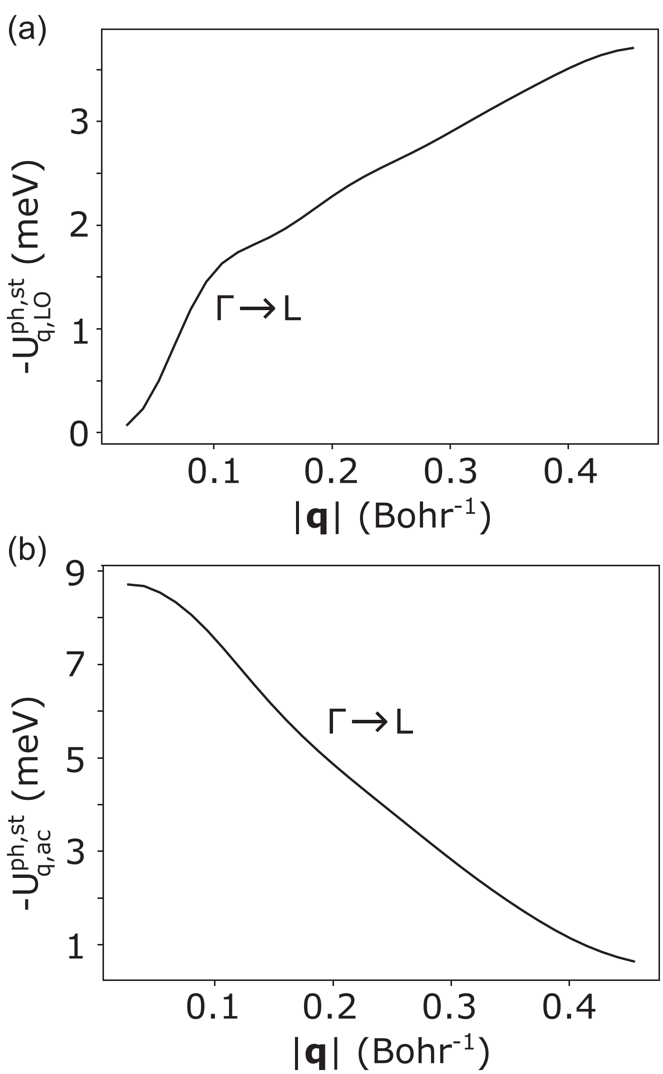

FIG. 11. Dependence of the short-range phonon-induced correction of the on-site Coulomb interaction on the phonon momentum, in the static limit. This is visualized for the LO phonon of GeTe, along the $\Gamma \rightarrow L$ path in reciprocal space (a), and for the strongest coupled acoustic phonon along the $\Gamma \rightarrow L$ path (b).

further contribute to superconductivity [86]. Indeed, it has previously been shown in the literature that a purely on-site phonon-mediated attraction between electrons can alone induce superconductivity, with appropriate retardation and strength [87]. Therefore our findings of a strongly attractive on-site interaction between electrons, which overcomes the repulsion already at low frequencies, as well as the existence of a net attractive nearest neighbor interaction, already in the static limit, are strongly suggestive of the emergence of phonon-mediated superconductivity in GeTe, through the combination of the Fröhlich, deformation potential, and piezoelectric mechanisms. GeTe was already proposed to be a superconductor in 1969 by Allen and Cohen [69] based on a deformation potential mechanism, which we indeed find to provide a key contribution to the overall electron-electron attraction. Recent experiments have confirmed GeTe to be superconducting upon hole doping [70].

It is worth considering what makes GeTe unique within our formalism in terms of its ability to generate attractive electron-electron interactions compared to other semiconductors. The long-range Fröhlich coupling due to the single LO phonon in this material is not sufficient to lead to an overall attractive nearest-neighbor electron-electron interaction. As discussed for Eq. (32), LO phonons can, at most, cancel the electron-electron repulsion in the limit of $\epsilon_o \rightarrow \infty$, however, cannot result in an overall attractive interaction, in agreement with the prediction of Ref. [57]. Nevertheless, the strong dipolar electron-phonon coupling effectively screens out long-range electron-electron repulsion, and other mechanisms of electron coupling to phonons, including the deformation potential and piezoelectric mechanisms here, contribute to an additional attraction, which can flip the overall sign of the interaction between electrons. GeTe is known to exhibit significant piezoelectricity [76], resulting in important contributions from this mechanism of electron-phonon coupling. Additionally, the large values of its Born effective charges indicate a significant mixed ionic-covalent bonding character for the Ge-Te bond, and the covalent character is associated with strong deformation potential coupling [79]. Overall, it is the combination of the Fröhlich, piezoelectric, and deformation potential mechanisms for the electron-phonon interaction of GeTe, which are all substantial in this material, that results in an overall attraction between electrons.

VIII. DISCUSSION AND CONCLUSIONS

In this work, we have developed a theoretical and computational framework to account for phonon screening on electron-electron interactions, entirely from first principles. We account for short-range and long-range electron-phonon coupling on equal footing, and we have demonstrated simplifications of our expression in different limits, e.g., in the static limit, in the case where long-range electron-phonon interactions are described by the traditional Fröhlich model, and beyond. Moreover, we have demonstrated the connections of our formalism to applying a polaron transformation to a many-body electron-phonon Hamiltonian. Our theoretical scheme for including phonon effects in electronic interactions is directly compatible with *ab initio* downfolding schemes, which have grown in popularity for obtaining the properties of strongly-correlated materials from first principles [1–4].

We have applied our computational framework to MgO and GeTe, and in both cases we find significant phonon-induced renormalization of the electron-electron interactions, particularly for on-site Coulomb terms. This results mostly from short-range electron-phonon interactions based on the deformation potential mechanism, which, despite their fast decay, still lead to substantial nearest-neighbor attraction in GeTe. The interplay of this mechanism with long-range electron-phonon coupling screens out repulsive electron-electron interactions and leads to an overall attraction, which could provide an explanation for superconductivity in this system.

Our theoretical work could have important implications for accurately predicting the electronic phase diagrams of diverse materials and interpreting experiments. *Ab initio* downfolding casts the problem of describing the electronic structure of a material in the form of an extended Hubbard model (see Eq. (2)), which generally allows capturing complex phases such as charge density waves, spin density waves, and d-wave superconductivity depending on the values of the parameters t, U, V [87,88]. Therefore our approach to obtain the potentially strong phonon-induced renormalization of the Coulomb terms could significantly reshape theoretically predicted phase diagrams. The impact of long-range electron-phonon coupling, which our approach has incorporated into *ab initio* downfolding for the first time, would be particularly pronounced here, as this interaction can greatly renormalize the nearest-neighbor Coulomb interaction V (see our examples of MgO and GeTe), which can often determine the electronic phase of a material [87,88]. An implication of our work relevant to experiment includes the potential emergence of superconductivity in GeTe, due to static nearest-neighbor and retarded on-site attractive electron-electron interactions mediated by phonons. The renormalization of the Coulomb terms will also affect the transport properties of materials, particularly in the Mott insulator regime, where the conductivity can depend sensitively on the U, V values [89,90].

ACKNOWLEDGMENTS

The authors are thankful to Marvin L. Cohen for helpful and inspiring discussions. The authors also express their gratitude to the anonymous referees for pointing out the regime of validity of Eq. (27), which led to modifications in Appendix B and the addition of Appendix C. This material is based upon work supported by the U.S. Department of Energy, Office of Science, National Quantum Information Science Research Centers, Superconducting Quantum Materials and Systems Center (SQMS) under Contract No. DE-AC02-07CH11359. We are grateful for support from NASA Ames Research Center. A.M.A. thanks the Physics Department and the Oden Institute for Computational Engineering and Sciences at The University of Texas at Austin for their support. C.J.N.C. and M.R.F. acknowledge support from the UK Engineering and Physical Sciences Research Council (EPSRC). Z.L. acknowledges the support by the U.S. National Science Foundation (NSF) CAREER Award under Grant No. DMR-2440763. V.V. was supported by the National Science Foundation (NSF) CAREER award through Grant No. DMR-1945098. This research used resources of the National Energy Research Scientific Computing Center, a DOE Office of Science User Facility supported by the Office of Science of the U.S. Department of Energy under Contract No. DE-AC02-05CH11231 using NERSC Awards No. HEP-ERCAP0029167 and No. DDR-ERCAP0029710.

DATA AVAILABILITY

The data that support the findings of this article are not publicly available. The data are available from the authors upon reasonable request.

APPENDIX A: DETAILED DERIVATION OF THE PHONON CORRECTION TO THE COULOMB INTERACTION

The general 4-center Coulomb interaction appearing in downfolded Hamiltonians can be written as

$$U_{i\mathbf{R}j\mathbf{R}'k\mathbf{R}''l\mathbf{R}'''}(\omega) = \int_V d\mathbf{r}_1 d\mathbf{r}_2 \phi^*_{i\mathbf{R}}(\mathbf{r}_1)\phi_{i\mathbf{R}'}(\mathbf{r}_2)W(\mathbf{r}_1,\mathbf{r}_2;\omega)\phi^*_{k\mathbf{R}''}(\mathbf{r}_1)\phi_{l\mathbf{R}'''}(\mathbf{r}_2). \tag{A1}$$

Taking $W = W^{\mathrm{el}} + W^{\mathrm{ph}}$, the integral becomes

$$U_{i\mathbf{R}j\mathbf{R}'k\mathbf{R}''l\mathbf{R}'''}(\omega) = U^{\mathrm{el}}_{i\mathbf{R}j\mathbf{R}'k\mathbf{R}''l\mathbf{R}'''}(\omega) + U^{\mathrm{ph}}_{i\mathbf{R}j\mathbf{R}'k\mathbf{R}''l\mathbf{R}'''}(\omega), \tag{A2}$$

where the electronically screened Coulomb interaction is given by

$$U^{\mathrm{el}}_{i\mathbf{R}j\mathbf{R}',k\mathbf{R}''l\mathbf{R}'''}(\omega) = \langle \phi_{i\mathbf{R}}\phi_{j\mathbf{R}'}|W^{\mathrm{el}}(\omega)|\phi_{k\mathbf{R}''}\phi_{l\mathbf{R}'''}\rangle, \tag{A3}$$

and the phonon-screened term is

$$U^{\mathrm{ph}}_{i\mathbf{R}j\mathbf{R}',k\mathbf{R}''l\mathbf{R}'''}(\omega) = \langle \phi_{i\mathbf{R}}\phi_{j\mathbf{R}'}|W^{\mathrm{ph}}(\omega)|\phi_{k\mathbf{R}''}\phi_{l\mathbf{R}'''}\rangle. \tag{A4}$$

We now focus on developing the expression for $U^{\mathrm{ph}}_{i\mathbf{R}j\mathbf{R}',k\mathbf{R}''l\mathbf{R}'''}(\omega)$. Using Eq. (11) for W^{ph} and resolving the identity in the position basis, we have

$$U^{\mathrm{ph}}_{i\mathbf{R}j\mathbf{R}',k\mathbf{R}''l\mathbf{R}'''}(\omega) = \int d\mathbf{r}_1 d\mathbf{r}_2 \phi^*_{i\mathbf{R}}(\mathbf{r}_1)\phi^*_{j\mathbf{R}'}(\mathbf{r}_2)W^{\mathrm{ph}}(\mathbf{r}_1,\mathbf{r}_2;\omega)\phi_{k\mathbf{R}''}(\mathbf{r}_1)\phi_{l\mathbf{R}'''}(\mathbf{r}_2), \tag{A5}$$

which gives

$$U^{\mathrm{ph}}_{i\mathbf{R}j\mathbf{R}',k\mathbf{R}''l\mathbf{R}'''}(\omega) = \sum_{\mathbf{q}\nu} D_{\mathbf{q}\nu}(\omega)\int d\mathbf{r}_1 d\mathbf{r}_2 \phi^*_{i\mathbf{R}}(\mathbf{r}_1)\phi^*_{j\mathbf{R}'}(\mathbf{r}_2) g_{\mathbf{q}\nu}(\mathbf{r}_1) g^*_{\mathbf{q}\nu}(\mathbf{r}_2)\phi_{k\mathbf{R}''}(\mathbf{r}_1)\phi_{l\mathbf{R}'''}(\mathbf{r}_2). \tag{A6}$$

The integral factorizes and so we have

$$U^{\mathrm{ph}}_{i\mathbf{R}j\mathbf{R}',k\mathbf{R}''l\mathbf{R}'''}(\omega) = \sum_{\mathbf{q}\nu} D_{\mathbf{q}\nu}(\omega)\int d\mathbf{r}_1 \phi^*_{i\mathbf{R}}(\mathbf{r}_1) g_{\mathbf{q}\nu}(\mathbf{r}_1)\phi_{k\mathbf{R}''}(\mathbf{r}_1)\int d\mathbf{r}_2 \phi^*_{j\mathbf{R}'}(\mathbf{r}_2) g^*_{\mathbf{q}\nu}(\mathbf{r}_2)\phi_{l\mathbf{R}'''}(\mathbf{r}_2). \tag{A7}$$

The typical electron-phonon vertex integral is given by

$$\int d\mathbf{r}_1 \phi^*_{i\mathbf{R}}(\mathbf{r}_1) g_{\mathbf{q}\nu}(\mathbf{r}_1)\phi_{k\mathbf{R}''}(\mathbf{r}_1) = \int d\mathbf{r}_1 \phi^*_{i\mathbf{0}}(\mathbf{r}_1-\mathbf{R}) g_{\mathbf{q}\nu}(\mathbf{r}_1)\phi_{k\mathbf{0}}(\mathbf{r}_1-\mathbf{R}''), \tag{A8}$$

where we have used the property that $\phi_{i\mathbf{R}}(\mathbf{r}_1) = \phi_{i\mathbf{0}}(\mathbf{r}_1-\mathbf{R})$. Further, changing variables to $\mathbf{r} = \mathbf{r}_1 - \mathbf{R}$, we have

$$\int d\mathbf{r}_1 \phi^*_{i\mathbf{0}}(\mathbf{r}_1-\mathbf{R}) g_{\mathbf{q}\nu}(\mathbf{r}_1)\phi_{i\mathbf{0}}(\mathbf{r}_1-\mathbf{R}'') = \int d\mathbf{r} \phi^*_{i\mathbf{0}}(\mathbf{r}) g_{\mathbf{q}\nu}(\mathbf{r}+\mathbf{R})\phi_{i\mathbf{0}}(\mathbf{r}-(\mathbf{R}''-\mathbf{R})) = g_{ii\mathbf{q}\nu}(\mathbf{R},\mathbf{R}''), \tag{A9}$$

where

$$g_{mn\mathbf{q}\nu}(\mathbf{R},\mathbf{R}'') = \langle\phi_{m\mathbf{R}}|\, g_{\mathbf{q}\nu}\,|\phi_{n\mathbf{R}''}\rangle = \sum_{n'm'\mathbf{k}} e^{-i\mathbf{k}\cdot(\mathbf{R}''-\mathbf{R})} e^{i\mathbf{q}\cdot\mathbf{R}} w^{\dagger}_{mn'}(\mathbf{k}+\mathbf{q}) g_{n'm'\nu}(\mathbf{k},\mathbf{q}) w_{m'n}(\mathbf{k}), \tag{A10}$$

w_{mn} being Wannier rotation matrices, and $g_{nm\nu}(\mathbf{k},\mathbf{q})$ the electron-phonon matrix element in the Bloch basis. Therefore we have

$$U^{\mathrm{ph}}_{i\mathbf{R}j\mathbf{R}',k\mathbf{R}''l\mathbf{R}'''}(\omega) = \sum_{\mathbf{q}\nu} D_{\mathbf{q}\nu}(\omega) g_{ik\mathbf{q}\nu}(\mathbf{R},\mathbf{R}'') g^*_{lj\mathbf{q}\nu}(\mathbf{R}''',\mathbf{R}'), \tag{A11}$$

and finally we have

$$U^{\mathrm{ph}}_{i\mathbf{R}j\mathbf{R}',k\mathbf{R}''l\mathbf{R}'''}(\omega) = \sum_{\mathbf{q}\nu} g_{ik\mathbf{q}\nu}(\mathbf{R},\mathbf{R}'') g^*_{lj\mathbf{q}\nu}(\mathbf{R}''',\mathbf{R}')\left(\frac{1}{\omega-\omega_{\mathbf{q}\nu}+i\eta} - \frac{1}{\omega+\omega_{\mathbf{q}\nu}-i\eta}\right). \tag{A12}$$

The density-density interaction is given by the following matrix element

$$U^{\mathrm{ph}}_{i\mathbf{R}j\mathbf{R}'}(\omega) \equiv U^{\mathrm{ph}}_{i\mathbf{R}j\mathbf{R}',i\mathbf{R}j\mathbf{R}'}(\omega) \tag{A13}$$

which in the static limit $\omega = 0$ reduces to

$$U^{\mathrm{ph,st}}_{i\mathbf{R}j\mathbf{R}'} = -2\sum_{\mathbf{q}\nu}\frac{g_{ii\mathbf{q}\nu}(\mathbf{R}) g^*_{jj\mathbf{q}\nu}(\mathbf{R}')}{\omega_{\mathbf{q}\nu}}, \tag{A14}$$

where here we define

$$g_{mn\mathbf{q}\nu}(\mathbf{R}) \equiv g_{mn\mathbf{q}\nu}(\mathbf{R},\mathbf{R}) = \sum_{n'm'\mathbf{k}} e^{i\mathbf{q}\cdot\mathbf{R}} w^{\dagger}_{mn'}(\mathbf{k}+\mathbf{q}) g_{n'm'\nu}(\mathbf{k},\mathbf{q}) w_{m'n}(\mathbf{k}). \tag{A15}$$

Using the translational symmetry of the lattice, we have

$$U_{i\mathbf{R}j\mathbf{R}'} = U_{i\mathbf{0}j\mathbf{R}'-\mathbf{R}} \tag{A16}$$

and so

$$U^{\mathrm{ph,st}}_{i\mathbf{R}j\mathbf{R}'} = -2\sum_{\mathbf{q}\nu}\frac{g_{ii\mathbf{q}\nu}(\mathbf{0}) g^*_{jj\mathbf{q}\nu}(\mathbf{R}'-\mathbf{R})}{\omega_{\mathbf{q}\nu}}. \tag{A17}$$

By focusing on the on-site interaction, we find

$$U^{\mathrm{ph,st}}_{i\mathbf{R}i\mathbf{R}} = -2\sum_{\mathbf{q}\nu}\frac{|g_{ii\mathbf{q}\nu}(\mathbf{0})|^2}{\omega_{\mathbf{q}\nu}}. \tag{A18}$$

APPENDIX B: DERIVATION OF THE LONG-RANGE CONTRIBUTION TO U^{ph}

For brevity, below we drop band indices and we work in the static limit $\omega = 0$, however, the results immediately generalize to the case of finite ω. The long-range attractive electron-electron interaction due to phonons is written as (Eq. (A14))

$$U^{\mathrm{ph},\mathcal{L}}_{\mathbf{R}\mathbf{R}'}(\omega=0) = -2\sum_{\mathbf{q}\nu}\frac{g^{\mathcal{L}}_{\mathbf{q}\nu}(\mathbf{R}) g^{\mathcal{L}*}_{\mathbf{q}\nu}(\mathbf{R}')}{\omega_{\mathbf{q}\nu}}. \tag{B1}$$

Using the expression for the generalized Fröhlich vertex Eq. (20) gives

$$U^{\mathrm{ph},\mathcal{L}}_{\mathbf{R}\mathbf{R}'}(\omega=0) = -2\left(\frac{4\pi}{V}\right)^2 \sum_{\mathbf{q}\nu}\sum_{\kappa\kappa'}\left(\frac{1}{2N\omega^2_{\mathbf{q}\nu}}\right)\frac{1}{\sqrt{M_\kappa M_{\kappa'}}}\frac{(\mathbf{q}\cdot\mathbf{Z}_\kappa\cdot\mathbf{e}_{\kappa\nu}(\mathbf{q}))(\mathbf{q}\cdot\mathbf{Z}_{\kappa'}\cdot\mathbf{e}_{\kappa'\nu}(\mathbf{q}))}{(\mathbf{q}\cdot\epsilon_\infty\cdot\mathbf{q})^2}$$
$$\times \langle\phi_{i\mathbf{R}}(\mathbf{r})\phi_{j\mathbf{R}'}(\mathbf{r}')|\, e^{i\mathbf{q}\cdot(\mathbf{r}-\mathbf{r}')}\, |\phi_{i\mathbf{R}}(\mathbf{r})\phi_{j\mathbf{R}'}(\mathbf{r}')\rangle\,. \quad \text{(B2)}$$

First let us focus on the matrix element $\langle\phi_{i\mathbf{R}}(\mathbf{r})\phi_{j\mathbf{R}'}(\mathbf{r}')|\, e^{i\mathbf{q}\cdot(\mathbf{r}-\mathbf{r}')}\, |\phi_{i\mathbf{R}}(\mathbf{r})\phi_{j\mathbf{R}'}(\mathbf{r}')\rangle$. Written out in integral form, this factorizes as

$$\langle\phi_{i\mathbf{R}}(\mathbf{r})\phi_{j\mathbf{R}'}(\mathbf{r}')|\, e^{i\mathbf{q}\cdot(\mathbf{r}-\mathbf{r}')}\, |\phi_{i\mathbf{R}}(\mathbf{r})\phi_{j\mathbf{R}'}(\mathbf{r}')\rangle = \int d\mathbf{r} e^{i\mathbf{q}\cdot\mathbf{r}}|\phi_{i\mathbf{R}}(\mathbf{r})|^2 \int d\mathbf{r}' e^{-i\mathbf{q}\cdot\mathbf{r}'}|\phi_{j\mathbf{R}'}(\mathbf{r}')|^2. \quad \text{(B3)}$$

For well-localized Wannier functions, the corresponding form factors $F_i(\mathbf{q}) = \int d\mathbf{r}\, e^{i\mathbf{q}\cdot\mathbf{r}}|\phi_{i\mathbf{R}}(\mathbf{r})|^2$ are smooth and satisfy $F_i(\mathbf{q}) = e^{i\mathbf{q}\cdot\mathbf{R}}[1+\mathcal{O}(q^2)]$. Thus, to leading order in the long-wavelength regime, the matrix element reduces to $e^{i\mathbf{q}\cdot(\mathbf{R}-\mathbf{R}')}$.

We can thus write

$$U^{\mathrm{ph},\mathcal{L}}_{\mathbf{R}\mathbf{R}'}(\omega=0) = -2\left(\frac{4\pi}{V}\right)^2 \sum_{\mathbf{q}\nu}\sum_{\kappa\kappa'}\left(\frac{1}{2N\omega^2_{\mathbf{q}\nu}}\right)\frac{1}{\sqrt{M_\kappa M_{\kappa'}}}\frac{(\mathbf{q}\cdot\mathbf{Z}_\kappa\cdot\mathbf{e}_{\kappa\nu}(\mathbf{q}))(\mathbf{q}\cdot\mathbf{Z}_{\kappa'}\cdot\mathbf{e}_{\kappa'\nu}(\mathbf{q}))}{(\mathbf{q}\cdot\epsilon_\infty\cdot\mathbf{q})^2}e^{i\mathbf{q}\cdot(\mathbf{R}-\mathbf{R}')}. \quad \text{(B4)}$$

This expression is amenable to first-principles calculation, as everything that enters it may be obtained through DFPT calculations. However, we are now going to make a few well-justified approximations, which will greatly simplify its form.

The long-range Fröhlich interaction is controlled by the long-wavelength region of reciprocal space. In this regime, the optical phonon eigenvectors and frequencies are smooth functions of $|\mathbf{q}|$ (for fixed direction $\hat{\mathbf{q}}$), and may be expanded as

$$\mathbf{e}_{\kappa\nu}(\mathbf{q}) = \mathbf{e}_{\kappa\nu}(\mathbf{q}\to\mathbf{0}) + \mathcal{O}(q). \quad \text{(B5)}$$

To leading order in the long-wavelength limit, we therefore replace the polarization vectors by their $\mathbf{q}\to\mathbf{0}$ values,

$$\mathbf{e}_{\kappa\nu}(\mathbf{q}) \approx \mathbf{e}_{\kappa\nu}(\mathbf{q}\to\mathbf{0}), \quad \text{(B6)}$$

while retaining the explicit q dependence of the Fröhlich kernel. The neglected terms are higher order in q and contribute only subleading corrections to $U^{\mathrm{ph},\mathcal{L}}$.

We therefore have

$$U^{\mathrm{ph},\mathcal{L}}_{\mathbf{R}\mathbf{R}'}(\omega=0) = -2\left(\frac{4\pi}{V}\right)^2 \sum_{\mathbf{q}\nu}\sum_{\kappa\kappa'}\left(\frac{1}{2N\omega^2_{\mathbf{q}\nu}}\right)\frac{1}{\sqrt{M_\kappa M_{\kappa'}}}\frac{(\mathbf{q}\cdot\mathbf{Z}_\kappa\cdot\mathbf{e}_{\kappa\nu}(\mathbf{q}\to\mathbf{0}))(\mathbf{q}\cdot\mathbf{Z}_{\kappa'}\cdot\mathbf{e}_{\kappa'\nu}(\mathbf{q}\to\mathbf{0}))}{(\mathbf{q}\cdot\epsilon_\infty\cdot\mathbf{q})^2}e^{i\mathbf{q}\cdot(\mathbf{R}-\mathbf{R}')}. \quad \text{(B7)}$$

We now introduce the (mass-weighted) mode effective charge vector

$$\mathcal{Z}_{\nu,\alpha} \equiv \sum_{\kappa\beta}\frac{1}{\sqrt{M_\kappa}} Z_{\kappa,\alpha\beta}\, e_{\kappa\beta\nu}(\mathbf{q}\to\mathbf{0}), \quad \text{(B8)}$$

so that

$$\mathbf{q}\cdot\boldsymbol{\mathcal{Z}}_\nu = \sum_\kappa \frac{1}{\sqrt{M_\kappa}}\mathbf{q}\cdot\mathbf{Z}_\kappa\cdot\mathbf{e}_{\kappa\nu}(\mathbf{q}\to\mathbf{0}). \quad \text{(B9)}$$

We therefore obtain

$$U^{\mathrm{ph},\mathcal{L}}_{\mathbf{R}\mathbf{R}'}(\omega=0) = -\left(\frac{4\pi}{V}\right)^2 \sum_{\mathbf{q}\nu}\frac{1}{N\omega^2_{\mathbf{q}\nu}}\frac{|\mathbf{q}\cdot\boldsymbol{\mathcal{Z}}_\nu|^2}{(\mathbf{q}\cdot\boldsymbol{\epsilon}_\infty\cdot\mathbf{q})^2}e^{i\mathbf{q}\cdot(\mathbf{R}-\mathbf{R}')}. \quad \text{(B10)}$$

Writing $\mathbf{q} = |\mathbf{q}|\,\hat{\mathbf{q}}$, the quadratic contractions scale as

$$|\mathbf{q}\cdot\boldsymbol{\mathcal{Z}}_\nu|^2 \to |\mathbf{q}|^2\,|\hat{\mathbf{q}}\cdot\boldsymbol{\mathcal{Z}}_\nu|^2, \quad \text{(B11)}$$

$$(\mathbf{q}\cdot\boldsymbol{\epsilon}_\infty\cdot\mathbf{q})^2 \to |\mathbf{q}|^4\,(\hat{\mathbf{q}}\cdot\boldsymbol{\epsilon}_\infty\cdot\hat{\mathbf{q}})^2. \quad \text{(B12)}$$

Thus we are left with an overall factor $1/|\mathbf{q}|^2$ in the denominator. For simplicity, we denote the directional components $\hat{q}_\alpha$ simply by q_α in what follows. We therefore have

$$U^{\mathrm{ph},\mathcal{L}}_{\mathbf{R}\mathbf{R}'}(\omega=0) = -\left(\frac{4\pi}{V}\right)^2 \sum_{\mathbf{q}\nu}\frac{1}{N\omega^2_{\mathbf{q}\nu}}\cdot\frac{e^{i\mathbf{q}\cdot(\mathbf{R}-\mathbf{R}')}}{|\mathbf{q}|^2}\frac{|q_\alpha\mathcal{Z}_{\nu,\alpha}|^2}{\left(q_\alpha\epsilon^\infty_{\alpha\beta}q_\beta\right)^2}. \quad \text{(B13)}$$

This expression is amenable to first-principles computation, and is consistent with the ion part of the total dielectric function that was derived in the seminal review of Dolgov, Kirzhnits, and Maksymov [57], which the authors of Ref. [57] analyzed for the case of a two-atom unit cell. Here we will not use Eq. (B13) itself, but instead the limiting case of an isotropic system and of a system with mild anisotropy, which we derive in the following sections. Finally, we will show how for certain systems Eq. (B13) reduces to a simpler form that only requires knowledge of the dielectric constant and LO-TO splittings.

1. Long-range phonon-mediated interaction for an isotropic system

To make further progress from Eq. (B13), we assume that the long-wavelength interaction is isotropic, so that the dielectric tensor may be written as $\epsilon^{\infty}_{\alpha\beta} = \epsilon_{\infty}\delta_{\alpha\beta}$. In this limit,

$$\left(q_\alpha \epsilon^{\infty}_{\alpha\beta} q_\beta\right)^2 = \epsilon_{\infty}^2. \tag{B14}$$

Moreover, in an isotropic medium, the long-wavelength LO modes are characterized by a polarization parallel to $\mathbf{q}$, so that the associated mode effective charge is aligned with $\mathbf{q}$. The contraction then becomes independent of direction and reduces to

$$|q_\alpha \mathcal{Z}_{\nu,\alpha}|^2 = |\boldsymbol{\mathcal{Z}}_\nu|^2. \tag{B15}$$

The mode effective charge contributes to the long-range interaction only for LO modes. We therefore restrict the mode index to the LO branches, labeled by m. Given the smooth variation of the LO phonon frequencies in the long-wavelength limit, we substitute them by their $\mathbf{q} \to \mathbf{0}$ values, i.e., $\omega_{\mathbf{q}m} = \omega_{\mathrm{LO},m}$, which is also independent of the direction of $\mathbf{q}$ under the isotropy assumption. Using the identity $\frac{1}{r} = \frac{4\pi}{NV}\sum_{\mathbf{q}} \frac{e^{i\mathbf{q}\cdot\mathbf{r}}}{|\mathbf{q}|^2}$, we arrive at

$$U^{\mathrm{ph},\mathcal{L}}_{\mathbf{RR}'}(\omega = 0) = -\sum_m \left(\frac{4\pi}{V}\right) \frac{|\boldsymbol{\mathcal{Z}}_m|^2}{\epsilon_\infty\, \omega^2_{\mathrm{LO},m}} \frac{1}{\epsilon_\infty |\mathbf{R} - \mathbf{R}'|}. \tag{B16}$$

Finally, defining

$$\gamma^2 = \left(\frac{4\pi}{V}\right) \sum_m \frac{|\boldsymbol{\mathcal{Z}}_m|^2}{\epsilon_\infty\, \omega^2_{\mathrm{LO},m}}, \tag{B17}$$

we can write this in the compact form

$$U^{\mathrm{ph},\mathcal{L}}_{\mathbf{RR}'}(\omega = 0) = -\frac{\gamma^2}{\epsilon_\infty |\mathbf{R} - \mathbf{R}'|}. \tag{B18}$$

2. Long-range phonon-mediated interaction for a mildly anisotropic system

For an anisotropic system, we retain the full dielectric tensor $\epsilon^{\infty}_{\alpha\beta}$ in Eq. (B13). In this case, the long-range interaction acquires a directional dependence through the factor $|q_\alpha \mathcal{Z}_{\nu,\alpha}|^2/(q_\alpha \epsilon^{\infty}_{\alpha\beta} q_\beta)^2$. For use in an effective isotropic model, we define an isotropized long-range interaction by replacing this directional dependence by its orientational average over the unit sphere. This is a good approximation for systems with modest dielectric anisotropy. Restricting again to the LO branches labeled by m and using $\omega_{\mathbf{q}m} \simeq \omega_{\mathrm{LO},m}$ in the long-wavelength limit, Eq. (B13) becomes

$$U^{\mathrm{ph},\mathcal{L}}_{\mathbf{RR}'}(\omega = 0) \simeq -\left(\frac{4\pi}{V}\right)^2 \sum_m \frac{1}{N\omega^2_{\mathrm{LO},m}} \left[\int \frac{d\Omega}{4\pi} \frac{|q_\alpha \mathcal{Z}_{m,\alpha}|^2}{\left(q_\alpha \epsilon^{\infty}_{\alpha\beta} q_\beta\right)^2}\right] \sum_{\mathbf{q}} \frac{e^{i\mathbf{q}\cdot(\mathbf{R}-\mathbf{R}')}}{|\mathbf{q}|^2}. \tag{B19}$$

Using $\frac{1}{r} = \frac{4\pi}{NV}\sum_{\mathbf{q}} \frac{e^{i\mathbf{q}\cdot\mathbf{r}}}{|\mathbf{q}|^2}$, this yields the effective isotropic form

$$U^{\mathrm{ph},\mathcal{L}}_{\mathbf{RR}'}(\omega = 0) \simeq -\left(\frac{4\pi}{V}\right) \sum_m \frac{1}{\omega^2_{\mathrm{LO},m}} \left[\int \frac{d\Omega}{4\pi} \frac{|q_\alpha \mathcal{Z}_{m,\alpha}|^2}{\left(q_\alpha \epsilon^{\infty}_{\alpha\beta} q_\beta\right)^2}\right] \frac{1}{|\mathbf{R} - \mathbf{R}'|}. \tag{B20}$$

To retain a Coulomb-like screened form, we introduce an effective dielectric constant

$$\frac{1}{\epsilon_{\mathrm{eff}}} \equiv \int \frac{d\Omega}{4\pi} \frac{1}{q_\alpha \epsilon^{\infty}_{\alpha\beta} q_\beta}. \tag{B21}$$

We then define γ^2 as

$$\gamma^2 = \epsilon_{\mathrm{eff}} \left(\frac{4\pi}{V}\right) \sum_m \frac{1}{\omega^2_{\mathrm{LO},m}} \int \frac{d\Omega}{4\pi} \frac{|q_\alpha \mathcal{Z}_{m,\alpha}|^2}{\left(q_\alpha \epsilon^{\infty}_{\alpha\beta} q_\beta\right)^2}, \tag{B22}$$

so that the long-range interaction retains the compact Coulomb-like form

$$U^{\mathrm{ph},\mathcal{L}}_{\mathbf{RR}'}(\omega = 0) \simeq -\frac{\gamma^2}{\epsilon_{\mathrm{eff}}\, |\mathbf{R} - \mathbf{R}'|}. \tag{B23}$$

3. Simplification to an expression involving the LO-TO splittings

In some cases, it is possible to make an additional simplification in the definition of γ^2 and the final result for the phonon-mediated electron-electron interaction. We demonstrate this in the case of an isotropic material, however it is straightforward to generalize the discussion to an anisotropic system.

For certain materials, symmetry guarantees that the phonon eigenvectors at $\mathbf{q} \to \mathbf{0}$ are identical to those at $\mathbf{q} = \mathbf{0}$, even if the frequencies differ. In those cases, the longitudinal projection of the mode effective charge is related to the LO–TO splitting via [50]

$$\left(\frac{4\pi}{V}\right)\frac{|q_\alpha \mathcal{Z}_{\nu,\alpha}|^2}{q_\alpha \epsilon^\infty_{\alpha\beta} q_\beta} = \omega^2_{\mathrm{LO},\nu} - \omega^2_{\mathrm{TO},\nu}. \tag{B24}$$

Using this relation in the definition of γ^2 yields

$$\gamma^2 = \sum_m \frac{\omega^2_{\mathrm{LO},m} - \omega^2_{\mathrm{TO},m}}{\omega^2_{\mathrm{LO},m}}, \tag{B25}$$

and the phonon-mediated electron-electron interaction takes the simple form

$$U^{\mathrm{ph},\mathcal{L}}_{\mathbf{RR}'}(\omega = 0) = -\sum_m \left(\frac{\omega^2_{\mathrm{LO},m} - \omega^2_{\mathrm{TO},m}}{\omega^2_{\mathrm{LO},m}}\right)\frac{1}{\epsilon_\infty|\mathbf{R} - \mathbf{R}'|}. \tag{B26}$$

While this is a very convenient form for the Coulomb interaction, we emphasize again that it is only strictly valid when $\mathbf{e}(\mathbf{q} \to \mathbf{0}) = \mathbf{e}(\mathbf{q} = \mathbf{0})$. For MgO and GeTe this condition holds to excellent accuracy, as discussed in the following Appendix C, and hence Eq. (B26) may be used. In the more general case, γ^2 is computed directly from the Born effective charges and phonon eigenvectors through the mode effective charge defined in Eq. (B8).

APPENDIX C: VALIDITY OF EQS. (29) AND (B26) FOR MGO AND GETE

The simplified form of the long-range interaction, Eqs. (29) and (B26), relies on the condition that the phonon eigenvectors at long wavelength coincide with those at the Brillouin-zone center,

$$\mathbf{e}_\nu(\mathbf{q} \to 0) = \mathbf{e}_\nu(\mathbf{q} = 0), \tag{C1}$$

up to an overall phase and possible unitary rotations within degenerate subspaces. We verify this explicitly in MgO and GeTe by computing the overlap between mass-weighted phonon eigenvectors obtained from DFPT.

For a mode ν at $\mathbf{q} \to 0$ and a mode ν' at $\mathbf{q} = 0$, we define the squared overlap

$$\mathcal{O}_{\nu\nu'} = \left|\sum_{\kappa\alpha} e^*_{\kappa\alpha,\nu}(\mathbf{q} \to 0)\, e_{\kappa\alpha,\nu'}(\mathbf{q} = 0)\right|^2, \tag{C2}$$

where κ labels atoms and $\alpha = x, y, z$ Cartesian components. The eigenvectors are normalized according to the convention used in the DFPT output. This quantity is invariant under overall phase changes and provides a direct measure of the similarity between the two modes.

We also explicitly compare the values of γ^2 that determine the phonon-mediated interaction $-\gamma^2/(\epsilon \cdot r)$, when obtained from the general isotropic expression that involves the mode effective charges (Eq. (B17)), and the simpler expression involving the LO-TO splitting (Eq. (B25)), which relies on the approximation:

$$\left(\frac{4\pi}{V}\right)\frac{|q_\alpha \mathcal{Z}_{\nu,\alpha}|^2}{q_\alpha \epsilon^\infty_{\alpha\beta} q_\beta} = \omega^2_{\mathrm{LO},\nu} - \omega^2_{\mathrm{TO},\nu}. \tag{C3}$$

While the simplified expression of Eqs. (29) and (B26) holds for the systems we studied here, we emphasize that this should not be used without explicitly verifying that the phonon eigenvectors do not change between the $\mathbf{q} = \mathbf{0}$ point and the $\mathbf{q} \to \mathbf{0}$ region. This is only generally true for materials of certain symmetries and is not expected to hold in more complex cases, such as, for example, in cubic perovskites. In those cases, the Coulomb interaction will still be of the form $-\gamma^2/(\epsilon \cdot r)$, however, the strength of the electron-phonon coupling γ^2 should be evaluated using the more general expressions we derived for isotropic and mildly anisotropic materials, which involve the mode effective charges rather than the LO-TO splitting (Eqs. (B17) and (B22) for isotropic and anisotropic systems, respectively).

1. Direct comparison of phonon eigenvectors at q → 0 and q = 0 for MgO

In MgO, the optical modes at $\mathbf{q} = 0$ form a triply-degenerate subspace. In this case, individual eigenvectors at $\mathbf{q} = 0$ are not unique and may differ by unitary rotations within this subspace. A meaningful comparison is therefore obtained by projecting the long-wavelength eigenvector onto the entire degenerate subspace,

$$\sum_{\nu' \in \mathrm{deg.\ subspace}} \mathcal{O}_{\nu\nu'} \simeq 1. \tag{C4}$$

Numerically, we find that this sum is equal to 0.994 for the LO mode of MgO, demonstrating that the eigenvector at $\mathbf{q} \to 0$ lies almost entirely within the optical subspace at $\mathbf{q} = 0$. This confirms that $\mathbf{e}(\mathbf{q} \to 0)$ and $\mathbf{e}(\mathbf{q} = 0)$ coincide to excellent accuracy.

To make the procedure fully reproducible, we list in Table VI the DFPT eigenvector components used in the comparison. These correspond to the LO mode at $\mathbf{q} \to 0$ and the three degenerate optical modes at $\mathbf{q} = 0$.

TABLE VI. Mass-weighted phonon eigenvectors for MgO used in the overlap analysis. Components are listed in the order (Mg_x, Mg_y, Mg_z, O_x, O_y, O_z), as read from the DFPT eigenvector output files.

Mode	Mg_x	Mg_y	Mg_z	O_x	O_y	O_z
$q \to 0$ LO	−0.549839	0	0	0.835271	0	0
$q = 0$ opt. 1	0.411871	−0.256155	−0.026550	−0.741143	0.460940	0.047776
$q = 0$ opt. 2	0.203254	0.354090	−0.263184	−0.365747	−0.637170	0.473587
$q = 0$ opt. 3	−0.158140	−0.212043	−0.407416	0.284566	0.381563	0.733127

Using these values, the individual overlaps between the long-wavelength LO eigenvector and the three optical modes at $\mathbf{q} = 0$ are found to be 0.715, 0.174, and 0.105, respectively. Their sum, 0.994, is very close to unity, confirming that the long-wavelength eigenvector is essentially identical to the corresponding zone-center optical eigenvector, up to a rotation within the degenerate subspace.

This numerical result justifies the use of the relation

$$\left(\frac{4\pi}{V}\right)\frac{|q_\alpha \mathcal{Z}_{\nu,\alpha}|^2}{q_\alpha \epsilon^{\infty}_{\alpha\beta} q_\beta} = \omega^2_{\mathrm{LO},\nu} - \omega^2_{\mathrm{TO},\nu} \tag{C5}$$

for MgO. Using the more general isotropic expression that involves the mode-effective charges (Eq. (B17)) for γ^2, we find $\gamma^2 = 0.660$, whereas the simpler expression of Eq. (B25) involving the LO-TO splitting yields $\gamma^2 = 0.667$. Therefore the two values are in excellent agreement.

2. Direct comparison of phonon eigenvectors at q → 0 and q = 0 for GeTe

For GeTe, we verify the condition $\mathbf{e}(\mathbf{q} \to 0) \simeq \mathbf{e}(\mathbf{q} = 0)$ by explicitly comparing DFPT phonon eigenvectors. Since GeTe is mildly anisotropic, γ^2 is evaluated using the orientational averaging procedure outlined above. However, the validity of the LO–TO simplification depends only on the continuity of the eigenvectors between $\mathbf{q} \to 0$ and $\mathbf{q} = 0$. For brevity, we present the check for $\mathbf{q} \parallel x$; the same conclusion is obtained for other directions.

Here too we quantify the agreement using the squared overlap

$$\mathcal{O}_{\nu\nu'} = \left|\sum_{\kappa\alpha} e^*_{\kappa\alpha,\nu}(\mathbf{q} \to 0)\, e_{\kappa\alpha,\nu'}(\mathbf{q} = 0)\right|^2, \tag{C6}$$

with components listed in the order (Ge_x, Ge_y, Ge_z; Te_x, Te_y, Te_z).

At $\mathbf{q} = 0$, the optical modes at 8.6 meV are twofold degenerate, corresponding to two orthogonal polarizations. Therefore, as with MgO, we compute the total projection of the eigenvectors onto the degenerate subspace:

$$\sum_{\nu' \in \text{deg. subspace}} \mathcal{O}_{\nu\nu'} \simeq 1. \tag{C7}$$

Table VII lists the DFPT eigenvectors relevant for the comparison along $\mathbf{q} \parallel x$: the LO mode at $\mathbf{q} \to 0$ (mode 6 at 18.3 meV) and the two degenerate optical modes at $\mathbf{q} = 0$. Using these values, we find

$$\mathcal{O}_{(q\to 0)\mathrm{LO},\, q=0\,\mathrm{opt.}\,1} \simeq 7.6 \times 10^{-13}, \tag{C8}$$

$$\mathcal{O}_{(q\to 0)\mathrm{LO},\, q=0\,\mathrm{opt.}\,2} \simeq 0.999995, \tag{C9}$$

so that the projection onto the degenerate $q = 0$ subspace is $0.999995 \simeq 1$. This confirms that $\mathbf{e}(\mathbf{q} \to 0) \approx \mathbf{e}(\mathbf{q} = 0)$ to excellent accuracy for GeTe as well, thereby justifying the use of the LO–TO-based simplification when evaluating the long-range interaction. Using the anisotropic expression that involves the mode-effective charges [Eq. (B22)] for γ^2, we find $\gamma^2 = 0.649$, whereas the simpler expression of Eq. (B25) involving the LO-TO splitting yields $\gamma^2 = 0.78$, therefore slightly overestimating the long-range interaction.

APPENDIX D: CONNECTION BETWEEN DOWNFOLDING W^{ph} AND THE LANG-FIRSOV TRANSFORMATION

Here, we demonstrate the equivalence between the Lang-Firsov transformation and the static expression obtained for U^{ph} when downfolded in an extended Hubbard model. We work in a local basis and write the Hubbard model including an electron-phonon and a phonon term as

$$\begin{aligned} H = &\sum_{i\mathbf{R},j\mathbf{R}'} t_{i\mathbf{R},j\mathbf{R}'} a^\dagger_{i\mathbf{R}} a_{j\mathbf{R}'} + \frac{1}{2}\sum_{i\mathbf{R},j\mathbf{R}'} U_{i\mathbf{R},j\mathbf{R}'} a^\dagger_{i\mathbf{R}} a^\dagger_{j\mathbf{R}'} a_{j\mathbf{R}'} a_{i\mathbf{R}} \\ &+ \sum_{\mathbf{q}\nu} \omega_{\mathbf{q}\nu} b^\dagger_{\mathbf{q}\nu} b_{\mathbf{q}\nu} \\ &+ \sum_{i\mathbf{R}j\mathbf{R}'\mathbf{q}\nu} g_{ij\mathbf{q}\nu}(\mathbf{R},\mathbf{R}')(b_{\mathbf{q}\nu} + b^\dagger_{-\mathbf{q}\nu}) a^\dagger_{i\mathbf{R}} a_{j\mathbf{R}'}, \end{aligned} \tag{D1}$$

where we have dropped the spin indices for brevity; however, these are given explicitly in the formulas in the main part of the manuscript. This general Hamiltonian includes nonlocal scattering between $\mathbf{R}$ and $\mathbf{R}'$, caused by coupling to a single phonon, described by the matrix element of Eq. (A10). For $\mathbf{R} = \mathbf{R}'$, this expression yields $g(\mathbf{R})$ (Eq. (A15)).

Let us first consider the nonlocal electron-phonon coupling $\mathbf{R} \neq \mathbf{R}'$, which results in a modification of the hopping term

$$\sum_{i\mathbf{R},j\mathbf{R}'} (t_{i\mathbf{R},j\mathbf{R}'} + g_{ij\mathbf{q}\nu}(\mathbf{R},\mathbf{R}'))(b_{\mathbf{q}\nu} + b^\dagger_{-\mathbf{q}\nu})) a^\dagger_{i\mathbf{R}} a_{j\mathbf{R}'},$$

which describes a Su-Schrieffer-Heeger (SSH) mechanism [54,55] of electron-phonon coupling. Given the strongly localized nature of Wannier functions, which is the basis we employ here, we expect these nonlocal terms $\langle \phi_{m\mathbf{R}}|\, g_{\mathbf{q}\nu}\, |\phi_{n\mathbf{R}'}\rangle$ to be small compared to the local terms $g_{mn\mathbf{q}\nu}(\mathbf{R}) = \langle \phi_{m\mathbf{R}}|\, g_{\mathbf{q}\nu}\, |\phi_{n\mathbf{R}}\rangle$. We will therefore ignore them moving forward; however, it will be interesting to examine the impact of these terms from first principles within a downfolding context, as a part of future work.

TABLE VII. Mass-weighted phonon eigenvectors for GeTe used in the overlap analysis along $\mathbf{q} \parallel x$. Components are listed in the order (Ge_x, Ge_y, Ge_z; Te_x, Te_y, Te_z), as read from the DFPT eigenvector output files. Tiny $\sim 10^{-6}$ components reflect printing precision.

	Ge_x	Ge_y	Ge_z	Te_x	Te_y	Te_z
$q \to 0$ LO ($\mathbf{q} \parallel x$)	0.869047	0	0	−0.494730	0	0
$q = 0$ opt. 1	1×10^{-6}	0.870151	0	0	−0.492785	0
$q = 0$ opt. 2	0.870151	-1×10^{-6}	0	−0.492785	0	0

We now restrict the electron-phonon interaction to the local form

$$V_{ep} = \sum_{i\mathbf{R}\mathbf{q}\nu} g_{ii\mathbf{q}\nu}(\mathbf{R})(b_{\mathbf{q}\nu} + b^\dagger_{-\mathbf{q}\nu})a^\dagger_{i\mathbf{R}}a_{i\mathbf{R}}. \tag{D2}$$

We introduce the Lang-Firsov transformation on the Hamiltonian as

$$\bar{H} = e^S H e^{-S}, \tag{D3}$$

where

$$S = \sum_{i\mathbf{R}\mathbf{q}\nu} a^\dagger_{i\mathbf{R}}a_{i\mathbf{R}} \frac{g_{ii\mathbf{q}\nu}(\mathbf{R})}{\omega_{\mathbf{q}\nu}}(b^\dagger_{\mathbf{q}\nu} - b_{-\mathbf{q}\nu}). \tag{D4}$$

Application of this transformation results in the electronic operators as

$$\bar{a}_{i\mathbf{R}} = e^S a_{i\mathbf{R}} e^{-S} = a_{i\mathbf{R}} X_{i\mathbf{R}} \tag{D5a}$$

with

$$\bar{a}^\dagger_{i\mathbf{R}} = e^S a^\dagger_{i\mathbf{R}} e^{-S} = a^\dagger_{i\mathbf{R}} X^\dagger_{i\mathbf{R}}, \tag{D5b}$$

where

$$X_{i\mathbf{R}} = \exp\left(-\sum_{\mathbf{q}\nu} \frac{g_{ii\mathbf{q}\nu}(\mathbf{R})}{\omega_{\mathbf{q}\nu}}(b^\dagger_{\mathbf{q}\nu} - b_{-\mathbf{q}\nu})\right). \tag{D5c}$$

The phonon operators transform as

$$\bar{b}_{\mathbf{q}\nu} = b_{\mathbf{q}\nu} - \sum_{j\mathbf{R}'} \frac{g^*_{jj\mathbf{q}\nu}(\mathbf{R}')}{\omega_{\mathbf{q}\nu}} a^\dagger_{j\mathbf{R}'}a_{j\mathbf{R}'} \tag{D6a}$$

with

$$\bar{b}^\dagger_{\mathbf{q}\nu} = b^\dagger_{\mathbf{q}\nu} - \sum_{j\mathbf{R}'} \frac{g_{jj\mathbf{q}\nu}(\mathbf{R}')}{\omega_{\mathbf{q}\nu}} a^\dagger_{j\mathbf{R}'}a_{j\mathbf{R}'}. \tag{D6b}$$

The number operator is conserved since X_i is a unitary operator, i.e., $X^\dagger_{i\mathbf{R}}X_{i\mathbf{R}} = 1$, which means that

$$\bar{a}^\dagger_{i\mathbf{R}}\bar{a}_{i\mathbf{R}} = a^\dagger_{i\mathbf{R}}a_{i\mathbf{R}}. \tag{D7}$$

Additionally, we have

$$X^\dagger_{i\mathbf{R}} = \exp\left(\sum_{\mathbf{q}\nu} \frac{g_{ii\mathbf{q}\nu}(\mathbf{R})}{\omega_{\mathbf{q}\nu}}(b^\dagger_{\mathbf{q}\nu} - b_{-\mathbf{q}\nu})\right). \tag{D8}$$

Thus the similarity transformed Hamiltonian becomes

$$\begin{aligned}\bar{H} &= \sum_{i\mathbf{R},j\mathbf{R}'} t_{i\mathbf{R},j\mathbf{R}'} X_i^\dagger X_j a^\dagger_{i\mathbf{R}}a_{j\mathbf{R}'} + \frac{1}{2}\sum_{i\mathbf{R},j\mathbf{R}'} U_{i\mathbf{R},j\mathbf{R}'} a^\dagger_{i\mathbf{R}}a^\dagger_{j\mathbf{R}'}a_{j\mathbf{R}'}a_{i\mathbf{R}} \\ &\quad + \sum_{\mathbf{q}\nu}\omega_{\mathbf{q}\nu}\left(b^\dagger_{\mathbf{q}\nu} - \sum_{i\mathbf{R}}\frac{g_{ii\mathbf{q}\nu}(\mathbf{R})}{\omega_{\mathbf{q}\nu}}a^\dagger_{i\mathbf{R}}a_{i\mathbf{R}}\right) \\ &\quad \times \left(b_{\mathbf{q}\nu} - \sum_{j\mathbf{R}'}\frac{g^*_{jj\mathbf{q}\nu}(\mathbf{R}')}{\omega_{\mathbf{q}\nu}}a^\dagger_{j\mathbf{R}'}a_{j\mathbf{R}'}\right) \\ &\quad + \sum_{i\mathbf{R}\mathbf{q}\nu} g_{ii\mathbf{q}\nu}(\mathbf{R})\left(b_{\mathbf{q}\nu} + b^\dagger_{-\mathbf{q}\nu} - 2\sum_{j\mathbf{R}'}\frac{g^*_{jj\mathbf{q}\nu}(\mathbf{R}')}{\omega_{\mathbf{q}\nu}}a^\dagger_{j\mathbf{R}'}a_{j\mathbf{R}'}\right) \\ &\quad \times a^\dagger_{i\mathbf{R}}a_{i\mathbf{R}}.\end{aligned} \tag{D9}$$

The transformation results in a cancellation of the electron-phonon interaction, thereby giving

$$\begin{aligned}\bar{H} &= \sum_{i\mathbf{R},j\mathbf{R}'} t_{i\mathbf{R},j\mathbf{R}'} X_i^\dagger X_j a^\dagger_{i\mathbf{R}}a_{j\mathbf{R}'} \\ &\quad + \frac{1}{2}\sum_{i\mathbf{R},j\mathbf{R}'} U_{i\mathbf{R},j\mathbf{R}'} a^\dagger_{i\mathbf{R}}a^\dagger_{j\mathbf{R}'}a_{j\mathbf{R}'}a_{i\mathbf{R}} + \sum_{\mathbf{q}\nu}\omega_{\mathbf{q}\nu}b^\dagger_{\mathbf{q}\nu}b_{\mathbf{q}\nu} \\ &\quad + \sum_{i\mathbf{R}j\mathbf{R}'\mathbf{q}\nu}\frac{g_{ii\mathbf{q}\nu}(\mathbf{R})g^*_{jj\mathbf{q}\nu}(\mathbf{R}')}{\omega_{\mathbf{q}\nu}}a^\dagger_{i\mathbf{R}}a_{i\mathbf{R}}a^\dagger_{j\mathbf{R}'}a_{j\mathbf{R}'} \\ &\quad - 2\sum_{j\mathbf{R}'i\mathbf{R}\mathbf{q}\nu}\frac{g_{ii\mathbf{q}\nu}(\mathbf{R})g^*_{jj\mathbf{q}\nu}(\mathbf{R}')}{\omega_{\mathbf{q}\nu}}a^\dagger_{j\mathbf{R}'}a_{j\mathbf{R}'}a^\dagger_{i\mathbf{R}}a_{i\mathbf{R}}.\end{aligned} \tag{D10}$$

Now, using the anticommutation relations

$$\{a_{i\mathbf{R}}, a^\dagger_{j\mathbf{R}'}\} = \delta_{ij}\delta_{\mathbf{R}\mathbf{R}'}, \tag{D11}$$

we may rewrite the quartic terms generated by the Lang-Firsov transformation to give

$$\begin{aligned}\bar{H} &= \sum_{i\mathbf{R}}\left(t_{i\mathbf{R},i\mathbf{R}} - \sum_{\mathbf{q}\nu}\frac{|g_{ii\mathbf{q}\nu}(\mathbf{0})|^2}{\omega_{\mathbf{q}\nu}}\right)a^\dagger_{i\mathbf{R}}a_{i\mathbf{R}} + \sum_{i\neq j\mathbf{R}\mathbf{R}'} t_{i\mathbf{R},j\mathbf{R}'} \\ &\quad \times \exp\left(-\sum_{\mathbf{q}\nu}\frac{[g_{jj\mathbf{q}\nu}(\mathbf{R}') - g_{ii\mathbf{q}\nu}(\mathbf{R})]}{\omega_{\mathbf{q}\nu}}(b^\dagger_{\mathbf{q}\nu} - b_{-\mathbf{q}\nu})\right)a^\dagger_{i\mathbf{R}} \\ &\quad \times a_{j\mathbf{R}'} + \frac{1}{2}\sum_{i\mathbf{R},j\mathbf{R}'}\left(U_{i\mathbf{R},j\mathbf{R}'} - 2\sum_{\mathbf{q}\nu}\frac{g_{ii\mathbf{q}\nu}(\mathbf{R})g^*_{jj\mathbf{q}\nu}(\mathbf{R}')}{\omega_{\mathbf{q}\nu}}\right) \\ &\quad \times a^\dagger_{i\mathbf{R}}a^\dagger_{j\mathbf{R}'}a_{j\mathbf{R}'}a_{i\mathbf{R}} + \sum_{\mathbf{q}\nu}\omega_{\mathbf{q}\nu}b^\dagger_{\mathbf{q}\nu}b_{\mathbf{q}\nu},\end{aligned} \tag{D12}$$

where we have used $|g_{ii\mathbf{q}\nu}(\mathbf{R})|^2 = |g_{ii\mathbf{q}\nu}(\mathbf{0})|^2$. The result of the transformation is the effective interactions

$$\tilde{t}_{i\mathbf{R},i\mathbf{R}} = t_{i\mathbf{R},i\mathbf{R}} - \sum_{\mathbf{q}\nu}\frac{|g_{ii\mathbf{q}\nu}(\mathbf{0})|^2}{\omega_{\mathbf{q}\nu}} \tag{D13a}$$

with the off-site interaction modulated by

$$\tilde{t}_{i\mathbf{R},j\mathbf{R}'} = t_{i\mathbf{R},j\mathbf{R}'}$$

$$\times \exp\left[-\sum_{\mathbf{q}\nu}\frac{[g_{jj\mathbf{q}\nu}(\mathbf{R}')-g_{ii\mathbf{q}\nu}(\mathbf{R})]}{\omega_{\mathbf{q}\nu}}(b^\dagger_{\mathbf{q}\nu}-b_{-\mathbf{q}\nu})\right] \tag{D13b}$$

and the two-body interaction is renormalized as

$$\tilde{U}_{i\mathbf{R},j\mathbf{R}'} = U_{i\mathbf{R},j\mathbf{R}'} - 2\sum_{\mathbf{q}\nu}\frac{g_{ii\mathbf{q}\nu}(\mathbf{R})g^*_{jj\mathbf{q}\nu}(\mathbf{R}')}{\omega_{\mathbf{q}\nu}}. \tag{D13c}$$

As we can see, the contribution to the two-body term is exactly the static phonon-screened contribution so we may write

$$\tilde{U}_{i\mathbf{R},j\mathbf{R}'} = U_{i\mathbf{R},j\mathbf{R}'} + U^{\mathrm{ph,st}}_{i\mathbf{R},j\mathbf{R}'}. \tag{D14}$$

Using these effective interactions, the similarity transformed Hamiltonian takes the form

$$\bar{H} = \sum_{i\mathbf{R},j\mathbf{R}'}\tilde{t}_{i\mathbf{R},j\mathbf{R}'}a^\dagger_{i\mathbf{R}}a_{j\mathbf{R}'} + \frac{1}{2}\sum_{i\mathbf{R},j\mathbf{R}'}\tilde{U}_{i\mathbf{R},j\mathbf{R}'}a^\dagger_{i\mathbf{R}}a^\dagger_{j\mathbf{R}'}a_{j\mathbf{R}'}a_{i\mathbf{R}} + \sum_{\mathbf{q}\nu}\omega_{\mathbf{q}\nu}b^\dagger_{\mathbf{q}\nu}b_{\mathbf{q}\nu}. \tag{D15}$$

Assuming a coherent decoupling of the phonon and electronic states, we may evaluate the temperature dependent trace of the off-site hopping term by

$$\tilde{t}_{i\mathbf{R},j\mathbf{R}'}(T) \approx t_{i\mathbf{R},j\mathbf{R}'}\exp\left[-\sum_{\mathbf{q}\nu}\frac{|g_{jj\mathbf{q}\nu}(\mathbf{R}')-g_{ii\mathbf{q}\nu}(\mathbf{R})|^2}{\omega^2_{\mathbf{q}\nu}}\left(N_{\mathbf{q}\nu}(T)+\frac{1}{2}\right)\right]. \tag{D16}$$

[1] K. Nakamura, Y. Yoshimoto, R. Arita, S. Tsuneyuki, and M. Imada, Optical absorption study by *ab initio* downfolding approach: Application to GaAs, Phys. Rev. B **77**, 195126 (2008).

[2] Y. Matsuo, Y. Yoshimoto, Y. Nohara, and M. Imada, *Ab initio* low-dimensional physics opened up by dimensional downfolding: Application to LaFeAsO, J. Phys. Soc. Jpn. **79**, 12 (2010).

[3] R. Arita, H. Ikeda, S. Sakai, and M. T. Suzuki, *Ab initio* downfolding study of the iron-based ladder superconductor $BaFe_2S_3$, Phys. Rev. B **92**, 054515 (2015).

[4] H. Zheng, H. J. Changlani, K. T. Williams, B. Busemeyer, and L. K. Wagner, From real materials to model Hamiltonians with density matrix downfolding, Front. Phys. **6**, 43 (2018).

[5] H. Q. Pham, M. R. Hermes, and L. Gagliardi, Periodic electronic structure calculations with the density matrix embedding theory, J. Chem. Theory Comput. **16**, 130 (2020).

[6] N. P. Bauman and K. Kowalski, Coupled cluster downfolding theory: Towards universal many-body algorithms for dimensionality reduction of composite quantum systems in chemistry and materials science, Mater. Theory **6**, 17 (2022).

[7] L. P. Weisburn, M. Cho, M. Bensberg, O. R. Meitei, M. Reiher, and T. V. Voorhis, Multiscale embedding for quantum computing, J. Chem. Theory Comput. **21**, 4591 (2025).

[8] F. Aryasetiawan, M. Imada, A. Georges, G. Kotliar, S. Biermann, and A. I. Lichtenstein, Frequency-dependent local interactions and low-energy effective models from electronic structure calculations, Phys. Rev. B **70**, 195104 (2004).

[9] L. Muechler, D. I. Badrtdinov, A. Hampel, J. Cano, M. Rösner, and C. E. Dreyer, Quantum embedding methods for correlated excited states of point defects: Case studies and challenges, Phys. Rev. B **105**, 235104 (2022).

[10] Y. Chang, E. G. van Loon, B. Eskridge, B. Busemeyer, M. A. Morales, C. E. Dreyer, A. J. Millis, S. Zhang, T. O. Wehling, L. K. Wagner, and M. Rösner, Downfolding from *ab initio* to interacting model Hamiltonians: Comprehensive analysis and benchmarking of the DFT+cRPA approach, npj Comput. Mater. **10**, 129 (2024).

[11] K. Yoshimi, T. Tsumuraya, and T. Misawa, *Ab initio* derivation and exact diagonalization analysis of low-energy effective Hamiltonians for β–X[Pd(dmit)$_2$]$_2$, Phys. Rev. Res. **3**, 043224 (2021).

[12] T. Botzung and P. Nataf, Exact diagonalization of SU (N) Fermi-Hubbard models, Phys. Rev. Lett. **132**, 153001 (2024).

[13] F. Ma, W. Purwanto, S. Zhang, and H. Krakauer, Quantum Monte Carlo calculations in solids with downfolded Hamiltonians, Phys. Rev. Lett. **114**, 226401 (2015).

[14] Y. Yoshida, N. Takemori, and W. Mizukami, *Ab initio* extended Hubbard model of short polyenes for efficient quantum computing, J. Chem. Phys. **161**, 084303 (2024).

[15] A. M. Alvertis, A. Khan, and N. M. Tubman, Ground states of strongly-correlated materials on quantum computers using *ab initio* downfolding, Phys. Rev. Appl. **23**, 044028 (2025).

[16] M. Hirayama, T. Misawa, T. Ohgoe, Y. Yamaji, and M. Imada, Effective Hamiltonian for cuprate superconductors derived from multiscale *ab initio* scheme with level renormalization, Phys. Rev. B **99**, 245155 (2019).

[17] T. Ohgoe, M. Hirayama, T. Misawa, K. Ido, Y. Yamaji, and M. Imada, *Ab initio* study of superconductivity and inhomogeneity in a Hg-based cuprate superconductor, Phys. Rev. B **101**, 045124 (2020).

[18] E. Been, W. S. Lee, H. Y. Hwang, Y. Cui, J. Zaanen, T. Devereaux, B. Moritz, and C. Jia, Electronic structure trends across the rare-earth series in superconducting infinite-layer nickelates, Phys. Rev. X **11**, 011050 (2021).

[19] M. T. Schmid, J. B. Morée, R. Kaneko, Y. Yamaji, and M. Imada, Superconductivity studied by solving *ab initio* low-energy effective Hamiltonians for carrier doped $CaCuO_2$, $Bi_2Sr_2CuO_6$, $Bi_2Sr_2CaCu_2O_8$, and $HgBa_2CuO_4$, Phys. Rev. X **13**, 041036 (2023).

[20] G. Mazza, M. Rösner, L. Windgätter, S. Latini, H. Hübener, A. J. Millis, A. Rubio, and A. Georges, Nature of symmetry breaking at the excitonic insulator transition: Ta_2NiSe_5, Phys. Rev. Lett. **124**, 197601 (2020).

[21] K. Yoshimi, T. Misawa, T. Tsumuraya, and H. Seo, Comprehensive *ab initio* investigation of the phase diagram of quasi-one-dimensional molecular solids, Phys. Rev. Lett. **131**, 036401 (2023).

[22] A. Schobert, J. Berges, E. G. C. P. van Loon, M. A. Sentef, S. Brener, M. Rossi, and T. O. Wehling, *Ab initio* electron-lattice downfolding: Potential energy landscapes, anharmonicity, and molecular dynamics in charge density wave materials, SciPost Phys. **16**, 046 (2024).

[23] F. Giustino, S. G. Louie, and M. L. Cohen, Electron-phonon renormalization of the direct band gap of diamond, Phys. Rev. Lett. **105**, 265501 (2010).

[24] G. Antonius, S. Poncé, P. Boulanger, M. Côté, and X. Gonze, Many-body effects on the zero-point renormalization of the band structure, Phys. Rev. Lett. **112**, 215501 (2014).

[25] B. Monserrat, E. A. Engel, and R. J. Needs, Giant electron-phonon interactions in molecular crystals and the importance of nonquadratic coupling, Phys. Rev. B **92**, 140302 (2015).

[26] A. Marini, *Ab initio* finite-temperature excitons, Phys. Rev. Lett. **101**, 106405 (2008).

[27] A. M. Alvertis, R. Pandya, L. A. Muscarella, N. Sawhney, M. Nguyen, B. Ehrler, A. Rao, R. H. Friend, A. W. Chin, and B. Monserrat, Impact of exciton delocalization on exciton-vibration interactions in organic semiconductors, Phys. Rev. B **102**, 081122 (2020).

[28] T. A. Huang, M. Zacharias, D. K. Lewis, F. Giustino, and S. Sharifzadeh, Exciton-phonon interactions in monolayer germanium selenide from first principles, J. Phys. Chem. Lett. **12**, 3802 (2021).

[29] M. F. Bishop and A. W. Overhauser, Phonon-mediated electron-electron interaction in real space, Phys. Rev. B **23**, 3627 (1981).

[30] W.-K. Tse and S. D. Sarma, Phonon-induced many-body renormalization of the electronic properties of graphene, Phys. Rev. Lett. **99**, 236802 (2007).

[31] Y. Nomura and R. Arita, *Ab initio* downfolding for electron-phonon-coupled systems: Constrained density-functional perturbation theory, Phys. Rev. B **92**, 245108 (2015).

[32] G. Giovannetti, M. Casula, P. Werner, F. Mauri, and M. Capone, Downfolding electron-phonon Hamiltonians from *ab initio* calculations: Application to K_3 picene, Phys. Rev. B **90**, 115435 (2014).

[33] E. G. C. P. van Loon, J. Berges, and T. O. Wehling, Downfolding approaches to electron-ion coupling: Constrained density-functional perturbation theory for molecules, Phys. Rev. B **103**, 205103 (2021).

[34] J. Berges, N. Girotto, T. Wehling, N. Marzari, and S. Poncé, Phonon self-energy corrections: To screen, or not to screen, Phys. Rev. X **13**, 041009 (2023).

[35] C. Yue, Y. Nomura, K. Prassides, and P. Werner, Instability of the $Pa\overline{3}$ fulleride Cs_3C_{60} at ambient pressure and superconducting state of the fcc phase, Phys. Rev. B **108**, L220508 (2023).

[36] C. Verdi and F. Giustino, Fröhlich electron-phonon vertex from first principles, Phys. Rev. Lett. **115**, 176401 (2015).

[37] W. H. Sio, C. Verdi, S. Poncé, and F. Giustino, *Ab initio* theory of polarons: Formalism and applications, Phys. Rev. B **99**, 235139 (2019).

[38] N. Marzari, A. A. Mostofi, J. R. Yates, I. Souza, and D. Vanderbilt, Maximally localized Wannier functions: Theory and applications, Rev. Mod. Phys. **84**, 1419 (2012).

[39] M. Romanova, G. Weng, A. Apelian, and V. Vlček, Dynamical downfolding for localized quantum states, npj Comput. Mater. **9**, 126 (2023).

[40] G. Strinati, Application of the Green's functions method to the study of the optical properties of semiconductors, Riv. Nuovo Cim. **11**, 1 (1988).

[41] M. Rohlfing and S. G. Louie, Electron-hole excitations in semiconductors and insulators, Phys. Rev. Lett. **81**, 2312 (1998).

[42] M. Rohlfing and S. G. Louie, Electron-hole excitations and optical spectra from first principles, Phys. Rev. B **62**, 4927 (2000).

[43] J. Deslippe, G. Samsonidze, D. A. Strubbe, M. Jain, M. L. Cohen, and S. G. Louie, BerkeleyGW: A massively parallel computer package for the calculation of the quasiparticle and optical properties of materials and nanostructures, Comput. Phys. Commun. **183**, 1269 (2012).

[44] A. Canestraight, Z. Huang, L. Lin, and V. Vlcek, Renormalization of states and quasiparticles in many-body downfolding, J. Chem. Phys. **163**, 024114 (2025).

[45] C. J. C. Scott and G. H. Booth, Rigorous screened interactions for realistic correlated electron systems, Phys. Rev. Lett. **132**, 076401 (2024).

[46] G. Baym, Field-theoretic approach to the properties of the solid state, Ann. Phys. (NY) **14**, 1 (1961).

[47] L. Hedin, New method for calculating the one-particle Green's function with application to the electron-gas problem, Phys. Rev. **139**, A796 (1965).

[48] F. Giustino, Electron-phonon interactions from first principles, Rev. Mod. Phys. **89**, 015003 (2017).

[49] J. Ruhman, Comment on 2501.17230 and 2502.00103 "Phonon-mediated electron attraction in SrTiO3 via the generalized Frohlich and deformation potential mechanisms" and "Theory of *ab initio* downfolding with arbitrary range electron-phonon coupling", arXiv:2503.00041 [cond-mat.supr-con].

[50] X. Gonze and C. Lee, Dynamical matrices, Born effective charges, dielectric permittivity tensors, and interatomic force constants from density-functional perturbation theory, Phys. Rev. B **55**, 10355 (1997).

[51] G. D. Mahan, *Many-Particle Physics*, Physics of Solids and Liquids (Springer, New York, 2013).

[52] A. M. Alvertis, J. B. Haber, Z. Li, C. J. N. Coveney, S. G. Louie, M. R. Filip, and J. B. Neaton, Phonon screening and dissociation of excitons at finite temperatures from first principles, Proc. Natl. Acad. Sci. USA **121**, e2403434121 (2024).

[53] M. R. Filip, J. B. Haber, and J. B. Neaton, Phonon screening of excitons in semiconductors: Halide perovskites and beyond, Phys. Rev. Lett. **127**, 067401 (2021).

[54] W. P. Su, J. R. Schrieffer, and A. J. Heeger, Solitons in polyacetylene, Phys. Rev. Lett. **42**, 1698 (1979).

[55] A. J. Heeger, S. Kivelson, J. R. Schrieffer, and W. P. Su, Solitons in conducting polymers, Rev. Mod. Phys. **60**, 781 (1988).

[56] F. Giustino, M. L. Cohen, and S. G. Louie, Electron-phonon interaction using Wannier functions, Phys. Rev. B **76**, 165108 (2007).

[57] O. V. Dolgov, D. A. Kirzhnits, and E. G. Maksimov, On an admissible sign of the static dielectric function of matter, Rev. Mod. Phys. **53**, 81 (1981).

[58] H. P. H. Fröhlich and S. Zienau, XX properties of slow electrons in polar materials, London, Edinburgh, Dublin Philos. Mag. J. Sci. **41**, 221 (1950).

[59] W. H. Sio and F. Giustino, Unified *ab initio* description of Fröhlich electron-phonon interactions in two-dimensional and three-dimensional materials, Phys. Rev. B **105**, 115414 (2022).

[60] K. Hannewald, V. M. Stojanović, J. M. T. Schellekens, P. A. Bobbert, G. Kresse, and J. Hafner, Theory of polaron bandwidth narrowing in organic molecular crystals, Phys. Rev. B **69**, 075211 (2004).

[61] E. V. n. Boström, P. Helmer, P. Werner, and C. Verdozzi, Electron-electron versus electron-phonon interactions in lattice models: Screening effects described by a density functional theory approach, Phys. Rev. Res. **1**, 013017 (2019).

[62] Y.-h. Chan, M. H. Naik, J. B. Haber, J. B. Neaton, S. G. Louie, D. Y. Qiu, and F. H. da Jornada, Exciton–phonon coupling induces a new pathway for ultrafast intralayer-to-interlayer exciton transition and interlayer charge transfer in WS_2-MoS_2 heterostructure: A first-principles study, Nano Lett. **24**, 7972 (2024).

[63] F. Brown-Altvater, G. Antonius, T. Rangel, M. Giantomassi, C. Draxl, X. Gonze, S. G. Louie, and J. B. Neaton, Band gap renormalization, carrier mobilities, and the electron-phonon self-energy in crystalline naphthalene, Phys. Rev. B **101**, 165102 (2020).

[64] P. Giannozzi, S. Baroni, N. Bonini, M. Calandra, R. Car, C. Cavazzoni, D. Ceresoli, G. L. Chiarotti, M. Cococcioni, I. Dabo, A. Dal Corso, S. Fabris, G. Fratesi, S. de Gironcoli, R. Gebauer, U. Gerstmann, C. Gougoussis, A. Kokalj, M. Lazzeri, L. Martin-Samos, *et al.*, QUANTUM ESPRESSO: A modular and open-source software project for quantum simulations of materials, J. Phys.: Condens. Matter **21**, 395502 (2009).

[65] G. Pizzi, V. Vitale, R. Arita, S. Blügel, F. Freimuth, G. Géranton, M. Gibertini, D. Gresch, C. Johnson, T. Koretsune, J. Ibanez-Azpiroz, H. Lee, J. M. Lihm, D. Marchand, A. Marrazzo, Y. Mokrousov, J. I. Mustafa, Y. Nohara, Y. Nomura, L. Paulatto, *et al.*, Wannier90 as a community code: New features and applications, J. Phys.: Condens. Matter **32**, 165902 (2020).

[66] H. Lee, S. Poncé, K. Bushick, S. Hajinazar, J. Lafuente-Bartolome, J. Leveillee, C. Lian, J.-M. Lihm, F. Macheda, H. Mori, H. Paudyal, W. H. Sio, S. Tiwari, M. Zacharias, X. Zhang, N. Bonini, E. Kioupakis, E. R. Margine, and F. Giustino, Electron–phonon physics from first principles using the EPW code, npj Comput. Mater. **9**, 156 (2023).

[67] K. Nakamura, Y. Yoshimoto, Y. Nomura, T. Tadano, M. Kawamura, T. Kosugi, K. Yoshimi, T. Misawa, and Y. Motoyama, RESPACK: An *ab initio* tool for derivation of effective low-energy model of material, Comput. Phys. Commun. **261**, 107781 (2021).

[68] B. Monserrat, Correlation effects on electron-phonon coupling in semiconductors: Many-body theory along thermal lines, Phys. Rev. B **93**, 100301 (2016).

[69] P. B. Allen and M. L. Cohen, Carrier-concentration-dependent superconductivity in SnTe and GeTe, Phys. Rev. **177**, 704 (1969).

[70] M. Kriener, M. Sakano, M. Kamitani, M. S. Bahramy, R. Yukawa, K. Horiba, H. Kumigashira, K. Ishizaka, Y. Tokura, and Y. Taguchi, Evolution of electronic states and emergence of superconductivity in the polar semiconductor GeTe by doping valence-skipping indium, Phys. Rev. Lett. **124**, 047002 (2020).

[71] A. Jain, S. P. Ong, G. Hautier, W. Chen, W. D. Richards, S. Dacek, S. Cholia, D. Gunter, D. Skinner, G. Ceder, and K. A. Persson, Commentary: The Materials Project: A materials genome approach to accelerating materials innovation, APL Mater. **1**, 011002 (2013).

[72] K. Momma and F. Izumi, *VESTA3* for three-dimensional visualization of crystal, volumetric and morphology data, J. Appl. Cryst. **44**, 1272 (2011).

[73] D. R. Hamann, Optimized norm-conserving Vanderbilt pseudopotentials, Phys. Rev. B **88**, 085117 (2013).

[74] M. J. van Setten, M. Giantomassi, E. Bousquet, M. J. Verstraete, D. R. Hamann, X. Gonze, and G. M. Rignanese, The PSEUDODOJO: Training and grading a 85 element optimized norm-conserving pseudopotential table, Comput. Phys. Commun. **226**, 39 (2018).

[75] J. P. Perdew, K. Burke, and M. Ernzerhof, Generalized gradient approximation made simple, Phys. Rev. Lett. **77**, 3865 (1996).

[76] R. Shaltaf, E. Durgun, J.-Y. Raty, P. Ghosez, and X. Gonze, Dynamical, dielectric, and elastic properties of GeTe investigated with first-principles density functional theory, Phys. Rev. B **78**, 205203 (2008).

[77] P. Vogl, Microscopic theory of electron-phonon interaction in insulators or semiconductors, Phys. Rev. B **13**, 694 (1976).

[78] A. Chernikov, V. Bornwasser, M. Koch, S. Chatterjee, C. N. Böttge, T. Feldtmann, M. Kira, S. W. Koch, T. Wassner, S. Lautenschläger, B. K. Meyer, and M. Eickhoff, Phonon-assisted luminescence of polar semiconductors: Fröhlich coupling versus deformation-potential scattering, Phys. Rev. B **85**, 035201 (2012).

[79] M. L. Cohen and S. G. Louie, *Fundamentals of Condensed Matter Physics* (Cambridge University Press, Cambridge, 2016).

[80] T. J. H. Hele, B. Monserrat, and A. M. Alvertis, Systematic improvement of molecular excited state calculations by inclusion of nuclear quantum motion: A mode-resolved picture and the effect of molecular size, J. Chem. Phys. **154**, 244109 (2021).

[81] S. Poncé, J.-M. Lihm, and C.-H. Park, Verification and validation of zero-point electron-phonon renormalization of the bandgap, mass enhancement, and spectral functions, npj Comput. Mater. **11**, 117 (2025).

[82] J. Park, J.-J. Zhou, V. A. Jhalani, C. E. Dreyer, and M. Bernardi, Long-range quadrupole electron-phonon interaction from first principles, Phys. Rev. B **102**, 125203 (2020).

[83] Z. Chen, Y. Wang, S. N. Rebec, T. Jia, M. Hashimoto, D. Lu, B. Moritz, R. G. Moore, T. P. Devereaux, and Z.-X. Shen, Anomalously strong near-neighbor attraction in doped 1D cuprate chains, Science **373**, 1235 (2021).

[84] M. Jiang, Enhancing d-wave superconductivity with nearest-neighbor attraction in the extended Hubbard model, Phys. Rev. B **105**, 024510 (2022).

[85] C. Peng, Y. Wang, J. Wen, Y. S. Lee, T. P. Devereaux, and H.-C. Jiang, Enhanced superconductivity by near-neighbor attraction in the doped extended Hubbard model, Phys. Rev. B **107**, L201102 (2023).

[86] W.-C. Chen, Y. Wang, and C.-C. Chen, Superconducting phases of the square-lattice extended Hubbard model, Phys. Rev. B **108**, 064514 (2023).

[87] Z. Han, S. A. Kivelson, and H. Yao, Strong coupling limit of the Holstein-Hubbard model, Phys. Rev. Lett. **125**, 167001 (2020).

[88] S. Onari, R. Arita, K. Kuroki, and H. Aoki, Phase diagram of the two-dimensional extended Hubbard model: Phase transitions between different pairing symmetries when charge and spin fluctuations coexist, Phys. Rev. B **70**, 094523 (2004).

[89] S. Ejima and S. Nishimoto, Phase diagram of the one-dimensional half-filled extended Hubbard model, Phys. Rev. Lett. **99**, 216403 (2007).

[90] M. F. Craciun, G. Giovannetti, S. Rogge, G. Brocks, A. F. Morpurgo, and J. van den Brink, Evidence for the formation of a Mott state in potassium-intercalated pentacene, Phys. Rev. B **79**, 125116 (2009).